Materials Design for High-Safety Sodium-Ion Battery

Chao Yang, Sen Xin, Liqiang Mai,* and Ya You*

Sodium-ion batteries, with their evident superiority in resource abundance and cost, are emerging as promising next-generation energy storage systems for large-scale applications, such as smart grids and low-speed electric vehicles. Accidents related to fires and explosions for batteries are a reminder that safety is prerequisite for energy storage systems, especially when aiming for grid-scale use. In a typical electrochemical secondary battery, the electrical power is stored and released via processes that generate thermal energy, leading to temperature increments in the battery system, which is the main cause for battery thermal abuse. The investigation of the energy generated during the chemical/electrochemical reactions is of paramount importance for battery safety, unfortunately, it has not received the attention it deserves. In this review, the fundamentals of the heat generation, accumulation, and transportation in a battery system are summarized and recent key research on materials design to improve sodium-ion battery safety is highlighted. Several effective materials design concepts are also discussed. This review is designed to arouse the attention of researcher and scholars and inspire further improvements in battery safety.

1. Introduction

The award of 2019 Nobel Prize in Chemistry is jointly given to John B. Goodenough, M. Stanley Whittingham, and Akira Yoshino, recognizing their pioneering work on the essential intercalation electrode materials for lithium-ion batteries (LIBs). As an indispensable part of the modern society, LIBs have revolutionized our daily lives by making the world wireless and rechargeable. On the other hand, the limited lithium reserves

C. Yang, Prof. L. Mai, Prof. Y. You
State Key Laboratory of Advanced Technology for Materials Synthesis and Processing
Wuhan University of Technology
Wuhan 430070, P. R. China
E-mail: mlq518@whut.edu.cn; youya@whut.edu.cn

Prof. S. Xin
CAS Key Laboratory of Molecular Nanostructure and Nanotechnology
and Beijing National Laboratory for Molecular Sciences
Institute of Chemistry
Chinese Academy of Sciences (CAS)
Beijing 100190, P. R. China

Prof. L. Mai
Foshan Xianhu Laboratory of the Advanced Energy Science and Technology Guangdong Laboratory
Xianhu Hydrogen Valley
Foshan 528200, P. R. China

The ORCID identification number(s) for the author(s) of this article can be found under https://doi.org/10.1002/aenm.202000974.

and the relatively high cell cost raises concerns on the sustainable development of LIBs, especially in the large-scale energy storage area, which put specific requirements on the price cost, safety, and durability of the battery.[1] In addition to the concern over potential shortage of lithium, the incidents associated with fires and explosions of state-of-the-art LIBs are stimulating advanced strategies and new safe alternatives in recent years.

Sodium-ion batteries (SIBs), with identical internal components and working principles with LIBs, have been proposed as one of the most promising next-generation energy storage technology because of the evident advantages of low-cost and worldwide abundance of charge carriers.[2] Besides, the cost of SIBs could be further reduced by use of Co/Ni-free cathode materials[3] and aluminum current collector on the anode side since sodium does not alloy with aluminum.[4] In addition to the economic benefits, the configuration of SIBs offers a potentially safe way for batteries storage and transportation. Since Al current collector does not dissolve into electrolyte at a voltage of 0 V, shipping and storing SIBs which contain no energy (a fully discharged state) is potentially feasible.[5] Moreover, Dahn's group investigated the thermal stability of positive materials for SIBs and found that the desodiated $Na_{0.5}CrO_2$ cathode was less reactive than Li_0FePO_4 in nonaqueous electrolyte at elevated temperatures.[6] Robinson et al. found that the self-heating rate in a Na-ion pouch cell is significantly slower than that in a commercial $LiCoO_2$ (LCO) pouch cell and the thermal runaway process is less exothermic for Na-ion cells, indicating that SIBs could be a potentially safer option compared with LIBs.[7] However, the larger and heavier Na ions have poor kinetic characteristic in the host structure during insertion reaction process, so it may lead to rapid degradation of the host materials with exothermic reaction.[8–10] In addition, the higher solubility of solid electrolyte interphase (SEI) of SIBs resulting from lower Lewis acidity of sodium complex, indicates that the incomplete coverage of electrode may further lead to undesired side reactions, accelerating heat generation. The cathode materials reported so far, roughly including oxides, polyanions, organics, Prussian blue and its analogues, which have poor electronic/ionic conductivity, will bring issues to thermal diffusion as well.[11] So far, nonaqueous liquid electrolyte is still the primary option for SIBs because of wide electrochemical stable window, high ionic conductivity, and rapid mass transfer at the electrolyte-electrode interface, yet giving rise to safety hazards.[12] Recent

**ADVANCED
SCIENCE NEWS**
www.advancedsciencenews.com

**ADVANCED
ENERGY
MATERIALS**
www.advenergymat.de

works demonstrate that sharp temperature rise, huge volume expansion, massive gas generation, and even fire accident occur during the thermal runaway event for SIBs,[7,13–14] therefore, the thermal failure is still a critical issue to tackle for developing a reliable Na-ion battery system.[15–16]

Under normal working conditions, the storage and release of electric power in SIBs would inevitably be accompanied by heat generation. Moreover, operating or storing cells under abuse conditions, such as overcharge, fast charging, and unconventional high temperatures, also initiates heat production.[17–19] External protection devices, such as connecting current/temperature/voltage sensors, have been widely used in LIBs to protect the batteries from thermal runaway, which decreases the energy density of the battery pack and seems to be unreliable under abuse conditions.[20–22] Recently, Li et al. have summarized the thermal failure issues of SIBs and discussed how to select electrode and electrolyte to build a safer SIB.[8] In this review, we discuss the safety issue of SIBs by focusing on the intrinsic heat effect from materials perspectives as they are the root cause for the thermal failure of a battery, and propose strategies about how to diminish unnecessary heat sources and accelerate heat dissipation process in SIBs. First, we will provide an overview of the basic sources of heat generation, thermal runaway process and critical criteria for evaluating the safety for a Na-ion battery system. Furthermore, we will summarize some materials design strategies and concepts to alleviate the intrinsic thermal effect generated during normal and abuse operation conditions. We hope this review will stimulate more researchers to pay attention to this aspect, and inspire more efforts to conquer the safety issue of SIBs.

2. The Origins of Safety Issues in Sodium-Ion Batteries

2.1. Origins of Heat Generations in Sodium-Ion Batteries

To have a better understanding about thermal behaviors of SIBs, it is essential to gain fundamental knowledge about the major sources of heat generation. In a Na-ion battery, heat generates as a result of a series of reversible and irreversible electrochemical/chemical reactions, which could be classified into three types: reversible heat Q_r, polarization heat Q_p, and side reaction heat Q_s.[23–24] The origin of heat generations at each component in SIBs are summarized in **Figure 1**.

1) Reversible heat Q_r, generally, accounts for the reversible entropy changes ΔS of the active materials during electrochemical reactions. The amount of Q_r could be calculated according to Equation (1) once the ΔS is measured[25–26]

$$Q = I \frac{T\Delta S}{nF} = \frac{IT}{\partial T} \frac{\partial E}{\partial T} \tag{1}$$

where I is the applied current, T is the absolute temperature, n is the number of charges evolved in the electrochemical reaction, F is the Faraday's constant, E is the open circuit voltage of the battery at equilibrium, $\partial E/\partial T$ is the entropy change term. Whether the electrochemical process is endothermic or

Chao Yang received his M.S. degree in the School of Materials Science and Engineering at Wenzhou University in 2019. He is currently a Ph.D. candidate at Wuhan University of Technology. His research focuses on materials for high-performance and safe sodium ion battery.

Liqiang Mai is Chair Professor of Materials Science and Engineering at Wuhan University of Technology (WUT). He received his Ph.D. degree from WUT in 2004. He carried out his postdoctoral research in Prof. Zhonglin Wang's group at Georgia Institute of Technology in 2006–2007. He worked as advanced research scholar in the laboratory of Prof. Charles M. Lieber at Harvard University in 2008–2011 and the laboratory of Prof. Peidong Yang at University of California, Berkeley in 2017. His current research interests focus on new nanomaterials for electrochemical energy storage and micro/nano energy devices.

Ya You received her Ph.D. degree in Physical Chemistry from Institute of Chemistry, Chinese Academy of Sciences in July 2015. She worked with Prof. Arumugam Manthiram from 2015 to 2018 and then with Prof. John B. Goodenough from 2018 to 2019 as a postdoc fellow at the Department of Mechanical Engineering, the University of Texas at Austin. She joined Wuhan University of Technology as a full professor in 2019. Her research focuses on materials design for electrochemical energy storage systems, such as Li-ion and Na-ion batteries.

exothermic depends on the materials involved. For instance, the Q_r in graphite/$LiMn_2O_4$ and graphite/$LiFePO_4$ systems are negative during the discharge process (cooling effect), and positive during the charging process (heating effect), while that of the graphite/LCO system is reversed.[17] According to Equation (1), Q_r is related to I (C-rate) and ∂E.

ADVANCED
SCIENCE NEWS
www.advancedsciencenews.com

ADVANCED
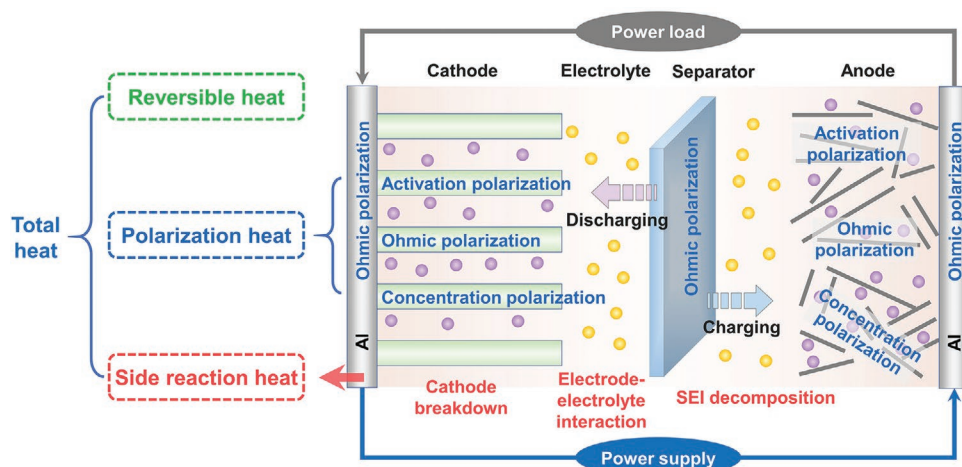ENERGY
MATERIALS
www.advenergymat.de

Figure 1. Schematic diagram of heat generation source in a sodium ion battery.

2) Polarization heat Q_p is one type of irreversible heat in a battery system. When a current (I) is applied to the cell, there is always a deviation between the cell operating potential (U_c) and the thermodynamic equilibrium potential (U_e), representing the voltage polarization of a battery. The additional energy consumption during charge and discharge process provokes the generation of heat. Q_p generated per unit time could be described by the following equation according to Li et al.[27]

$$Q_p = (U_c - U_e)I \qquad (2)$$

The causes of cell voltage polarization include ohmic polarization, activation polarization, and concentration polarization. Ohmic polarization (IR drop) refers to the internal potential drop induced by the ohmic resistance of a battery. The typical ohmic resistance of a battery is composed of the resistance passing electrons at the current collector and electrode materials, and the resistance passing Na^+ ions through electrolyte and separator. Activation polarization refers to the overpotential caused by overcoming the activation energy of the slowest step of the electrode electrochemical reaction. In a typical battery system, activation polarization arises from the electrochemical reaction process occurring at the electrode/electrolyte interfaces. Concentration polarization is the polarization originated from a faster reactants consumption rate than that of the mass transfer. The concentration polarization is associated with the limited diffusion and migration of Na^+ ions among electrodes and at the electrode surface.

3) Q_s represents another form of irreversible heat generated by undesired exothermic chemical reactions in batteries, including breakdown of SEI and the cathode–electrolyte interphase (CEI), reactions between electrolyte and electrode materials.[15,28–29] Generally, these side reactions are triggered at a critical temperature and the generated heat in turn raises the cell temperature, initiating thermal chain reactions.

Among all the sources for heat generation, the reversible heat Q_r could be endothermic or exothermic depending on the entropic coefficient of the electrochemical reaction while the irreversible heat Q_p and Q_s are exothermic. The reversible and irreversible heat generation rates are strongly affected by many factors, including charge/discharge rate, ambient temperature, state of charge (SOC), and electrode microstructure.[30–33] Typically, the reversible heat dominates at low C-rates while the ohmic heat dominates at high C-rates.[34] If the exothermic reactions in batteries go out of control, thermal runaway event would occur, which is one of the most catastrophic failure mode for SIBs.

2.2. Typical Thermal Runaway Process in Sodium-Ion Batteries

Thermal runaway occurs due to Heat-Temperature-Reaction (HTR) positive feedback loop. To be specific, heat generated in the cell increases the temperature, accelerates the exothermic reactions when the cell temperature reaches above a critical value. The exothermic reactions release more heat in return, forming the HTR loop. The continuously rising temperature may lead to fire or explosion accident, especially for large battery packs. Fundamental understanding of the causes and process of thermal runaway of SIBs is essential to guide the design of high safety materials for reliable and safe batteries. Robinson et al.[7] suggest that the thermal runaway process occurs in SIBs via identical mechanisms with that of LIBs. In general, the thermal runaway process is composed of three stages as shown in **Figure 2**: pre-stage, heat accumulation stage, and thermal abuse stage.

1) Pre-stage: Thermal runaway process is always initiated by excessive heating of the battery system. The amount of heat generated during charge/discharge process dynamically depends on the charge/discharge C-rates, kinetics of electrochemical reactions, ambient temperature, and its spatial distribution largely governed by the materials particle morphology, porosity, and the current density distributions.[35] The heat generation rate at various regions in cells is not uniform due to the nonuniformly distributed current during cycling. For instance, the temperature in pouch cells is higher at regions close to the tabs due to the higher current densities
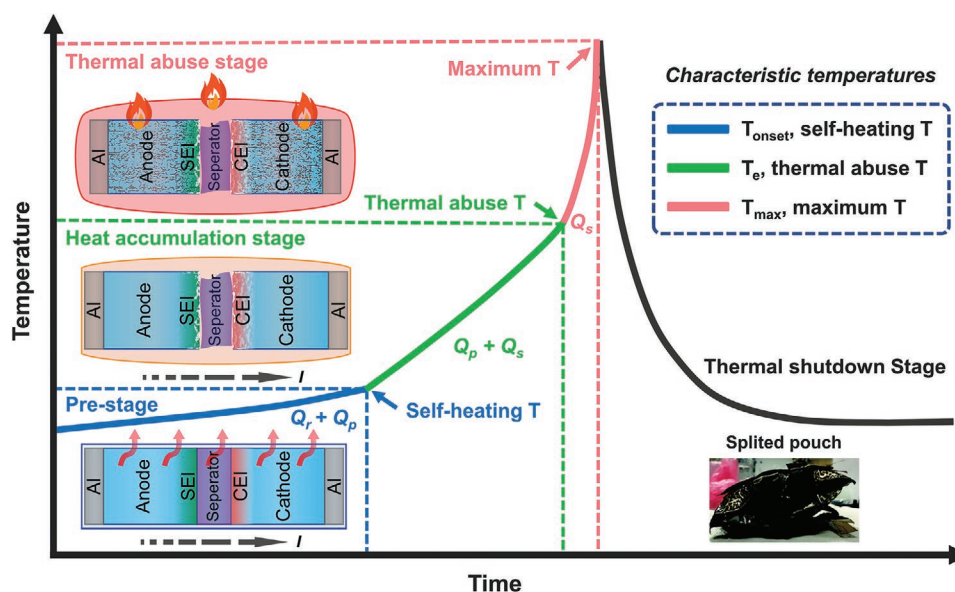
**ADVANCED
SCIENCE NEWS**
www.advancedsciencenews.com

**ADVANCED
ENERGY
MATERIALS**
www.advenergymat.de

Figure 2. Schematic illustration of the thermal runaway process of a Na-ion battery. Inset photo shows a splitted and parched sodium pouch cell after thermal runaway process. Reproduced with permission.[7] Copyright 2018, American Society of Mechanical Engineers.
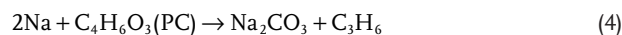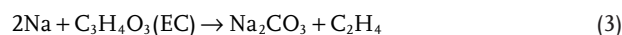
in these locations,[36] forming local hotspot where the onset of overheating normally starts. Apart from normal operation conditions, initial overheating of batteries also occurs at abuse conditions, including charging to a voltage exceed the designed value, exposure to high ambient temperature, external short circuit caused by wire connecting, and internal short circuit caused by cell flaw. Internal short circuit may happen in circumstances of mechanical failure, such as cell piercing, crushing, and falling. Once the cell temperature reaches to a onset value for thermal runaway, a self-heating process begins.

2) Heat accumulation stage: At this stage, temperature in the cell quickly increases as a result of exothermic chemical chain reactions, which are discussed in detail below.

i) Decomposition of SEI: Accelerating rate calorimetry (ARC) was employed to study the thermal runaway process of a Na-ion pouch cell (developed by Sharp Laboratories of Europe with a capacity of 3000 mA h) composed of layered oxide cathode, polypropylene separator, Na$^+$-conducting electrolyte, and hard carbon anode materials.[13–14] The first exothermic event initiated at ≈30 °C in the Na-ion cell is assigned to be the initial breakdown of the SEI at the hard carbon surface. Compared with a commercial LCO pouch cell with similar energy density, it takes less time to approach the first exothermic event and the onset temperature is slightly lower for the Na-ion cell, implying the SEI in Na-based system is less stable at elevated temperatures. Eshetu et al. systematically compared the compositions of SEI layer formed on sodiated and lithiated hard carbon. The electrolyte was 1 mol L^{-1} (M) NaPF$_6$ or LiPF$_6$ salt dissolving in mixed solution of ethylene carbonate (EC) and diethylene carbonate (DEC) (EC:DEC = 1:1 in weight). SEI layer formed in both Na- and Li-based systems contain a mixture of organic and inorganic species, including ROCO$_3$Na(Li), (Li)Na$_2$CO$_3$, RONa(Li), polyethylene oxide
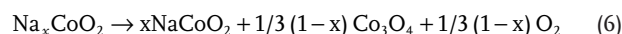
(PEO), NaF, etc.[37] Moreover, the content of organic compounds is higher in the SEI layer formed in Na$^+$-conducting electrolyte compared to its lithium counterpart, which might be the cause for its high sensitivity to temperature. The decomposition of organic species in SEI layer releases gases and further heat up the cell.

ii) Reactions between Anode and Electrolyte: Once the SEI layer decomposes, the exposed sodium metal cluster and inserted sodium ions would react with electrolyte to reform the SEI and release flammable gases. This process is also exothermic and increases the cell temperature further. Taking ester as an example, one form of the predictable reactions could be described as below

$$2Na + C_3H_4O_3 (EC) \rightarrow Na_2CO_3 + C_2H_4 \qquad (3)$$

$$2Na + C_4H_6O_3 (PC) \rightarrow Na_2CO_3 + C_3H_6 \qquad (4)$$

$$2Na + C_3H_6O_3 (DMC) \rightarrow Na_2CO_3 + C_2H_6 \qquad (5)$$

iii) Separator Meltdown: A traditional polyethylene (PE)/polypropylene (PP) separator would melt if the temperature rises above 130 °C, which makes the situation worse due to the internal short circuit caused by physical contact between positive and negative electrodes.[15] Liu et al. employed a ceramic polyethylene terephthalate (PET) separator with a melting point of 257 °C to avoid internal short circuit, nevertheless, a thermal runaway event still occurs.[38]

iv) Cathode Breakdown: At last, the continuously rising temperature leads to the decomposition of transition-metal layered oxide cathode materials in SIBs. Taking Na$_x$CoO$_2$ as an example, the decomposition process induced by heating is expected to proceed in the following manner

$$Na_xCoO_2 \rightarrow xNaCoO_2 + 1/3 (1-x) Co_3O_4 + 1/3 (1-x) O_2 \qquad (6)$$

ADVANCED
SCIENCE NEWS
www.advancedsciencenews.com

ADVANCED
ENERGY
MATERIALS
www.advenergymat.de

$$Co_3O_4 \rightarrow 3\,CoO + 0.5\,O_2 \qquad (7)$$

$$CoO \rightarrow Co + 0.5\,O_2 \qquad (8)$$

The decomposition of cathode materials has a strong exothermic property accompanied with oxygen generation. The accumulated oxygen further accelerates the decomposition of electrolyte, releasing more heat and raising the cell temperature. According to Robinson et al., the side reactions between the cathode materials and electrolyte are the leading cause of thermal runaway of SIBs.[7]

3) Thermal abuse stage: With adequate heat and oxygen accumulation in the system (Stage 2, green curve in Figure 2), thermal runaway bursts when the limiting oxygen index (LOI) of system satisfies the requirement for combustion of organic solvents in electrolyte (Stage 3, red curve in Figure 2). The index of entering the third stage is that the self-heating rate is greater than 10 °C min^{-1}.[29,39] Finally, the structure of the sodium ion battery would be seriously destroyed, causing a complete failure of the battery, as the charred and splitted pouch shown in the Figure 2.

2.3. Key Features for the Thermal Runaway Process

The key features in the thermal runaway event could be used for evaluating the safety degree of a battery as shown in Figure 2, which are discussed in details below.

1) Self-heating temperature T_{onset}: T_{onset} refers to the onset of a self-heating process, i.e., the beginning decomposition temperature of SEI. The HTR loop starts when the cell temperature is higher than T_{onset}. The reported T_{onset} of a Na-ion battery varies significantly from case to case, largely depending on the cell capacity, electrolyte composition, and working conditions. For example, the T_{onset} is between 30–50 °C for a 3000 mA h Na-ion pouch cell with 1 M NaPF$_6$ in EC:DEC (1:1 in weight) electrolyte,[7] but 166.3 °C for a 1000 mA h pouch cell using 1.0 M NaPF$_6$ dissolved in propylene carbonate (PC) and ethyl methyl carbonate (EMC) (1:1 in volume) with 2 wt% fluoroethylene carbonate (FEC) as electrolyte.[13]

2) Thermal abuse temperature T_e: T_e is the temperature at the turning point between the second stage and the third stage of a thermal runaway event, which is the highest point for normally working and convenient escape. At this critical point, the cell temperature shows an exponential increment. Batteries with higher T_e and longer time taken to reach T_e are believed to be more reliable.

3) Maximum temperature T_{max}: The maximum temperature during a thermal runaway process is another parameter closely related to the thermal behaviors for a battery. The Al current collectors would melt when the temperature goes up to a point of >660 °C, causing more internal short circuits and release more heat. The Al current collectors were observed to be intact on both electrodes in a Na-ion cell after thermal runaway, which indicates the T_{max} could not have exceeded 660 °C,[7] while a nickel manganese cobalt oxide cathode based Li-ion cell can exceed internal temperatures of at least 1085 °C.[40]

4) Heating power Q and total heat generation ΔH. The above-mentioned characteristic temperatures are closely related with the heat generated in cells, which is determined by the intrinsic property of electrode materials and electrolytes. Q determined the heating up rate for a cell and ΔH represented the overall energy released during the thermal runaway event. For a cell at 100% SOC, ΔH is predictable at an ideal condition that all the stored energy is released. For example, for a Na-ion cell with an energy density of 100 Wh kg^{-1}, ΔH equals $100 \times 3600/1000 = 360$ J g^{-1}.

5) Flammability of electrolyte, which is generally defined by self-extinguishing time (SET) or LOI. SET is used to describe how long an ignited sample continues to burn and it depends on whether the fire generates enough heat to evaporate adequate amounts of electrolyte to nourish the flame.[41] LOI is considered as a useful parameter to quantitatively evaluate the lowest concentration of O$_2$ to guarantee the combustion of electrolyte. Generally, if value of LOI is between 22 and 27, it is considered nonflammable. Value higher than 27 or below 22 is regarded as flame-retardant or flammable, respectively.[42] Therefore, the smaller value of SET or higher LOI is, the stronger the incombustibility is.

The development of high safety SIBs requires a comprehensive understanding of the thermal properties of key materials, which largely depends on the assistance of instruments and equipments. The high temperature synchrotron X-ray diffraction (HT-SXRD), thermogravimetry (TG) and differential scanning calorimetry (DSC) can be applied to study the phase transition and thermal decomposition of the positive and negative electrodes. Besides, DSC can be utilized to obtain heating power Q of cells. The thermal properties of electrolyte can be tested by DSC and critical oxygen index analyzer, while the thermal properties of the separator can be measured by DSC, TG, and differential thermal analysis. In addition, the temperature variations in cells can be monitored by multichannels temperature tester, infrared thermal imager, and ARC. It is essential to identify the above indicators qualitatively and quantitatively, from materials, cell, and pack levels, to gain fundamental knowledge about the thermal behaviors for SIBs, which provides guidance for safety evaluation, prediction, and thermal control strategies.

3. Strategies and Concepts for High-Safety Materials Design

The thermal behavior of a Na-ion battery is closely related to the intrinsic properties of each components, including positive and negative electrode materials, electrolytes, and separators. In this section, we will summarize various materials design approaches to reduce the safety hazards of SIBs.

3.1. Construction of Efficient Electrons, Ions, and Phonons Transport Networks

As we discussed in the last section, the thermal runaway event is always initiated by local overheating of a battery system. Under normal operating conditions, reducing irreversible

polarization heat Q_p generation and accelerating thermal diffusion are two effective means to prevent a hotspot in micro-scale. The voltage polarizations, including ohmic polarization, activation polarizations, and concentration polarizations (Figure 1), could be minimized by accelerating the kinetics of electrons and ions transfer among the electrodes, electrolyte, and electrode-electrolyte interfaces. The ionic and electronic conductivity are closely related to the electrode microstructure, in terms of particle size, interparticle or particle/current collector contact, porosity, active/inactive materials ratio, and thickness of the electrodes. In the previous work, it has been proved that the electronic conductivity can be enhanced by doping, coating, and 3D conductive network,[43–47] while the ions diffusion of the materials can also be enhanced by various nanostructures and decreased tortuosity (**Figure 3**a).[48–50] Readers could refer to a few references[51–53] for a good review of strategies to improve conduction in SIBs.

Moreover, heat dissipation would be critical under some extreme conditions, e.g., fast charging/discharging (large operation current I), as the Q_p is proportional to the square of current and hotspot may occur at areas with poor thermal conductivity. Thermal conductivity of metals primarily comes from the contribution of electrons, but most of compounds and semiconductors, especially the cathode materials, mostly originate from phonons contribution.[54] Therefore, constructing a synergetic system by carriers of electrons, ions and phonons is effective to simultaneously reduce the irreversible heat generation and accelerate heat transmission (Figure 3b). Consequently, it is integral to consider the influence of phonons, which account for a large proportion in heat transfer, on the thermal conductivity of SIBs materials. According to Debye formula,[55] the contribution of phonon to thermal conductivity (κ_p) can be described as

$$\kappa_p = \frac{1}{3} C_v \upsilon l_p \tag{9}$$

where C_v is the specific heat capacity of phonon, υ is velocity of free phonon, and l_p is mean free path of phonon motion. Among these parameters, C_v is related to the composition of the materials, which is almost regarded as a constant, while l_p depends on the microstructure of the materials.

κ_p could be effectively increased by reducing the intrinsic defects of materials. Phonon thermal conductivity corresponds to the transfer of a particle's vibrational energy to adjacent particles mainly by collision. Nevertheless, the introduction of defects will cause the scattering of wave lattice, which is equivalent to the reduction of the mean free path of the phonons. The long wavelength phonons scattering in heat transfer can be strongly enhanced by nanosized grain and grain boundary, while the phonons with short ones can be scattered by point defects and dislocations.[56] The above theory states that a simplified structure of materials can well enhance the phonon thermal conductivity. For polycrystals, phonons are more easily scattered due to smaller crystal size and more grain boundaries, impurities and defects, thus leading to a much smaller l_p than that of single crystals (Figure 3c). Therefore, the simplified crystal structure, e.g. monocrystallization of polycrystalline materials and crystallization of amorphous materials, can suppress phonon scattering. Taking $NaCoO_2$, one of the cathode material of SIBs, as a research objective, Fujita et al. studied the relationship between the crystallinity and thermal
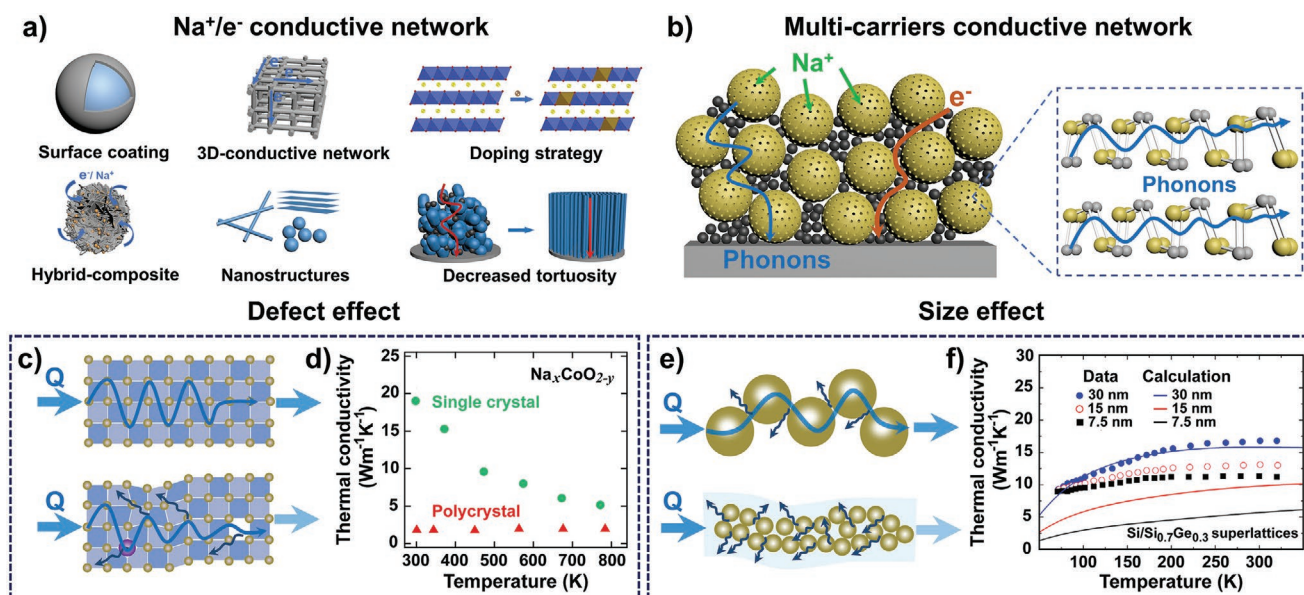

Figure 3. a) Schematic illustration of the strategies for building Na^+/e^- conductive networks. b) Schematic illustration of multicarriers conductive network, including Na^+, e^-, and phonons. c) Schematic illustration of phonons transportation and scattering in a perfect crystal lattice (top) and in distorted and defect lattice (bottom). d) The temperature dependence of the thermal conductivity of a Na_xCoO_{2-y} single crystal and a polycrystalline sample. Reproduced with permission.[57] Copyright 2001, American Institute Of Physics. e) Schematic illustration of phonons transmission and scattering among particles with large size is displayed in the top and small size is displayed in the bottom. f) Phonons thermal conductivity of Si/SiGe superlattices with different sizes. Reproduced with permission.[59] Copyright 2014, Elsevier.

**ADVANCED
SCIENCE NEWS**

www.advancedsciencenews.com

**ADVANCED
ENERGY
MATERIALS**

www.advenergymat.de

conductivity of the materials. It has been found that the in-plane thermal conductivity is determined to be about 19.0 Watt meter^{-1} Kelvin^{-1} (W m^{-1} K^{-1}) at 300 K for monocrystalline while 2.0 W m^{-1} K^{-1} for polycrystalline (Figure 3d).[57] The dominant component of thermal conductivity (κ) is κ_p in the Na$_x$CoO$_{2-y}$ sample and the difference of thermal conductivity between single crystal and polycrystalline samples is mainly due to the anisotropic effect. Li et al. employed TG/DSC, X-ray diffraction, Fourier transform infrared spectroscopy and nuclear magnetic resonance technologies to study the thermal conductivity of kaolinite nanoclay, and confirmed that the regularity of the microstructures can increase l_p. However, the phonons scattering increases based on the unreasonable geometry of silicon and aluminum oxygen units, thus limiting the average free path of phonons in kaolinite lattice.[58]

The size effect of materials is one of the considerable factors to affect the phonon thermal conductivity. Size control of particles is significant for developing high κ_p materials to decrease phonons scattering and improve the velocity of free phonons.[59] Thus, controlling the particle size can be recognized as a critical approach in the development of electrode materials of SIBs with high thermal conductivity (Figure 3e). Liang et al. linked the thermal conductivity with the system size by roughness, atomic vibration parameter, etc., and the agreement between the experimental and theoretical results indirectly confirmed that the thermoconductivity coefficient increased with the increment of size.[60] Dong et al. constructed Darcy–Brinkman model for phonons by considering the bulk friction and viscous friction of boundary, which further elaborated that bulk friction, related to the particle's size, takes a considerable part of the whole phonons resistance, even in sub-100 nm systems.[61] That work yielded the same results of the nonlinear proportional relationship between the size of materials and the thermal conductivity (Figure 3f). Additionally, the increase of the particle size can significantly reduce the specific surface area, thus inhibiting the side reaction between the electrode material and the electrolyte, and improving the initial coulombic efficiency (ICE).

It is also a considerable strategy to integrate materials with high phonon thermal conductivity to optimize the intrinsic thermal conductivity of materials. Meanwhile, it is more reasonable to optimize κ without sacrificing the electrochemical behavior for the SIBs system, so the conductivity of the auxiliary components also demands to be guaranteed. Graphene, silicon, metal carbides/nitrides, all possess good κ_p, which could be employed to improve the thermal conductivity of intrinsic materials through the synergistic effect of high thermal conductivity materials. Decreasing the incompatibility between components is equivalent to reduce the modulus mismatch, which would decrease the thermal interfacial resistance. This strategy can tolerate the scattering introduced by the boundaries, then weaken the total scattering intensity of the bulk phase, thereby improving the thermal conductivities of composites. Terao et al. fabricated the boron nitride nanotubes (BNNTs)/polyvinyl alcohol (PVA) composite fibers (<5 vol% BNNTs) by electrospinning, recording the highest thermal conductivity (0.54 W m^{-1} K^{-1}) compared with single component PVA.[62] The highest value was obtained when the films were elucidated along the long axis of the oriented BNNTs. Certainly, materials

with high electronic conductivity can also enhance the thermal conductivity synergism with phonons and electrons. Cui et al. incorporated 0.5 and 1 wt% raw multiwalled carbon nanotubes (rMWCNT) into an epoxy matrix to form epoxy/rMWCNT composites. The experimental results showed that, filled with 0.5 and 1 wt% r-MWCNTs, the thermal conductivity of epoxy/rMWCNT composites increase by 19% and 48%, respectively.[63]

The intrinsic thermal conductivity of polymer is relatively low, so binder/polymer-free electrode materials are considerable to increase the phonon thermal conductivity of electrodes. Yao et al.[64] proved that the thermal conductivity of single-walled carbon nanotubes (SWNT) decreased with increase of polyaniline. The thermal conductivity is 35 W m^{-1} K^{-1} for pure random SWNT material while about 17 W m^{-1} K^{-1} for 50 wt% polyaniline-50 wt% SWNT, which proved that polymer-free materials possess higher phonon thermal conductivity. Wu et al. investigated the organic-inorganic hybrid polyparaphenylene (PPP)/Li$_{0.5}$Ni$_{0.5}$Fe$_2$O$_4$ system.[65] The phonons thermal conductivity got maximum value when adding 0 wt% PPP, and it decreased with the increase of PPP.

The above available strategies can enhance the propagation of phonons in the crystal, and then enhance thermal conductivity in the bulk materials. The synergistical enhancement of electrons and phonons conductivity can be achieved by several strategies, including carbon layer coated active materials, single crystal active materials, and binder-free electrodes. The synergism of phonons, electrons and ions to weaken the generation of heat and accelerate the diffusion of heat will be of great significance for the development of safe battery system.

3.2. Thermally Stable Bulk Materials and Interfaces

When the self-heating process starts, Q_s becomes the dominating heat source in a battery system, which could be reduced by enhancing the thermal stability of bulk materials and interfaces. In a Na-ion cell, the onset temperature of the thermal runaway process is closely related to the stability of SEI on the surface of anode at elevated temperatures. Enhancing the thermal stability of SEI can improve the T_{onset} and expand the operation temperature range for SIBs. As shown in **Figure 4**a, one of the research directions for improving SEI stability is to optimize the composition by increasing inorganic species content and decreasing organic species content as excessive organic parts would result in high temperature sensitivity and severe side reactions caused by the porous characteristics.[15] Electrolyte additives, including NaPO$_2$F$_2$, vinylene carbonate (VC), FEC, and 1,3-propanesultone (PS) high temperature additives have been applied to form thin and stable SEI in SIBs.[66–70] Dahbi et al. studied the electrode/electrolyte interface formed on the surface of black phosphorus electrode by VC additive.[66] SEI formed in VC system is mainly composed of inorganic species, including NaF, Na$_x$PF$_y$, Na$_x$POF$_y$, etc., which originates from the decomposition of electrolyte (1 M NaPF$_6$ in EC: DEC (1:1, in volume)) and VC additives. In addition, the VC induced SEI layer is denser and thinner, compared to that in the VC-free electrolyte. Lu et al. investigated the surface structure and composition of SiC-Sb-C anode in FEC-free and FEC-containing electrolytes.[67] FEC preferentially decomposed on the particle
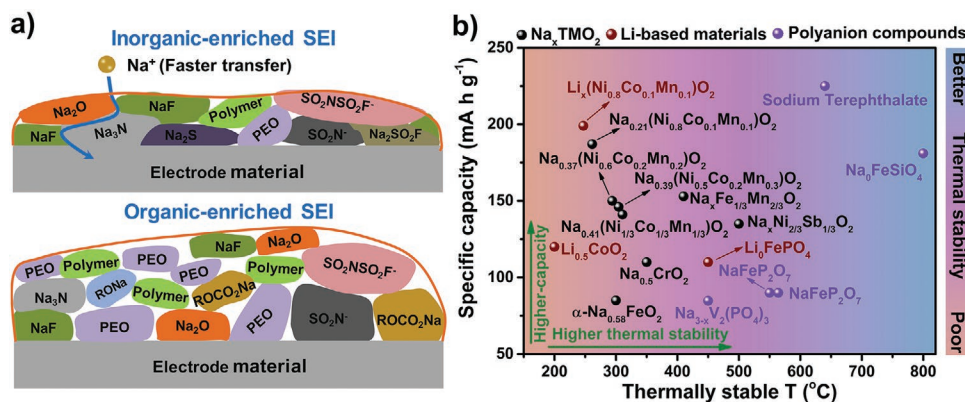
**ADVANCED
SCIENCE NEWS**

www.advancedsciencenews.com

**ADVANCED
ENERGY
MATERIALS**

www.advenergymat.de

Figure 4. a) Schematic illustration of an inorganic species enriched SEI (top) and organic-enriched SEI at the surface of anodes. b) A general comparison of specific capacity and thermal stability of various SIBs cathode materials (Datas of the thermal stability are obtained from DSC measurement of desodiated materials).[100–101,103–104,108,112,114,169–174]

surface because of higher reactivity of FEC than that of EC and DEC, and formed denser SEI films composed of NaF (inner) and Na_2CO_3, RONa (outer). FEC additive can change the morphology/structure and chemical composition of the passivation layer on the surface of the cycled electrode, so as to significantly reduce the irreversible capacity and improve the thermal stability. A large number of experiments have proved that a high content of inorganic materials in SEI will enhance the mechanical strength (Young's modulus), increase the compactness of the layer, and improve the heat resistance.[71–74] Ji et al. studied the SEI of porous carbon nanofiber-SnSb alloy (CNF-SnSb) in FEC and FEC-free electrolyte.[71] Analyzing from X-ray photoelectron spectroscopy, the thinner SEI formed in FEC-containing electrolyte is composed of NaF and Na polycarbonate, while the thicker one from FEC-free electrolyte is consisted of Na_2CO_3 and oxygen-rich carbonate, alkyl carbonate. Therefore, the morphology of SnSb fibers could be maintained after long-term cycling, illustrating that inorganic-enriched SEI shows high mechanical strength. This thin passivation layer can not only prevent further decomposition of electrolyte, but also provide a fast ion transport medium. Zheng et al. explored the Young's modulus of SEI on silicon surface by scanning probe microcopy.[72] Soft SEI parts, mainly composed of organic components, tend to grow on the outer layer of the SEI in VC additive system, while the inorganic-enriched inner SEI has a higher Young's modulus. Additionally, the stability of SEI in SIBs is associated with the types of salt.[75] Eshetu et al. comprehensively studied the thermal stability of SEI formed at the surface of Na metal in various carbonate-based electrolytes.[76] The order of onset temperature of exothermic process is NaClO4 > NaFTFSI > NaPF6 > NaTFSI > NaFSI in a fixed solvent (EC/PC), while EC/DMC > EC/DEC > EC/PC with a fixed sodium salt (NaPF6, NaClO4, or NaTFSI). The stronger solvation with EC and better thermal stability of NaPF6 than that of LiPF6 will form less acid in SIBs, thus reducing the Na_2CO_3 decomposition in SEI layer. Besides, the robustness and thickness of SEI are significantly influenced by the microstructure of anode materials. Li et al. regulated the pore species in waste cork-derived hard carbon anode materials and found that the platform capacity is closely related with the volume of closed

pores. An optimal annealing temperature of 1600 °C results in the largest volume of closed pores.[77] A decrease in the amount of open pores and defects reduces trapping of Na^+ by defects and interfacial reaction. As a result, a thin, smooth, and uniform SEI is formed.

Besides, optimizing the structure, composition, and density of SEI layer can preferentially alleviate the growth of dendrites, which is believed to be a major cause for internal short circuit and initiate thermal runaway.[78–81] Metal dendrite forms as a result of the uneven distribution of electrical field near the anode surface.[82] A porous and thick SEI layer should be avoided because it will impede the ion diffusion toward the anode surface, resulting in strong concentration gradient and accelerate the dendrite growth.[83] A stable, dense, and thin protective surface film is highly desired as it could reduce the undesired reactions between electrode and electrolyte. For example, a layer of artificial SEI layer, such as Al_2O_3, coated on the surface of the anode/cathode electrodes or functional polymeric membrane[84], is introduced to effectively inhibit the growth of dendrites.

In addition to SEI instability, the potential safety hazards of the anode also come from the sodium metal plating and the side reaction between the anode and binder or electrolyte. In order to achieve a high energy density, anode materials operating at a low potential is ideal for SIBs, e.g., hard-carbon materials. Nevertheless, there is a high possibility that sodium metal plates at the anode side if voltage is too low. Anode materials with moderate Na^+ ion insertion potential, such as $NaTi_2(PO_4)_3$,[85–87] $Na_2VTi(PO_4)_3$,[88] $Li_4Ti_5O_{12}$,[89] $Na_2Ti_6O_{13}$,[90–91] Sn,[92] $MnOOH$,[93] and $Na_2NiFe(CN)_6$,[85] show evident superiority in avoiding Na metal deposition. The vigorous chemical reactions between sodiated anode and electrolytes under elevated temperatures should be carefully studied. Jiang et al. found that $Na_2Ti_2(PO_4)_3$ anode material exhibits two exothermic peaks at 323.3 and 295.4 °C and release less total heat of 347 J g^{-1} compared with hard carbon in the carbonate electrolyte (EC: DEC).[86] Rudola et al. demonstrated that sodiated $Na_2Ti_6O_{13}$ anode (discharged to 0.5 V) can stabilize up to 500 °C.[90] The side-reaction heat of anode can be effectively reduced by decreasing the specific

**ADVANCED
SCIENCE NEWS**

www.advancedsciencenews.com

**ADVANCED
ENERGY
MATERIALS**

www.advenergymat.de

surface area of anode, reducing the amount of binder, and optimizing the binder composition.[94–95] According to Zhu et al., negative electrodes with polyimide (PI) as binder show enhancement in the electrochemical performance.[96] Besides, PI binder is thermally stable up to 500 °C with Si anode.

As for the thermal stability of separator, the commercial Celgard separator will encounter heat shrinkage approximately at 130 °C, which may cause internal short circuit. The heat resistance of separator can be strengthened by coating inorganic ceramic layer, filling gel in pores, components regulation, or combination with inorganic compound on nanofiber, etc.[97] Goodenough's group reported a ternary polymer composite polyvinylidene-fluoride-co-hexafluoropropylene (PVDF-HFP)/polyvinylpyrrolidone (PVP)/Sb_2O_3 as a membrane of battery.[98] The polymer composite-PVDF-HFP (45 wt%)/PVP (25 wt%)/Sb_2O_3 (30 wt%) is stable against sodium metals, easy to manufacture at low cost, and blocks sodium dendrites in long charge/discharge cycles. Moreover, its melting temperature is increased to at least 250 °C, which makes it suitable for medium and high temperature energy storage/conversion devices. Other researches on separators design from the perspective of micropores-closed function to tackle the thermal issue are discussed in Section 3.4.

Cathode breakdown would also lead to a strong exothermic behavior. Particularly, sodium layered transition metal oxide (Na_xTMO_2, TM = transition metal) materials may release oxygen at a deep charge state and high temperature, which potentially leads to catastrophic explosion. High-nickel oxides have the poorest stability among Na_xTMO2 materials, mainly caused by the oxidation of Ni^{3+} to Ni^{4+} in the state of high deintercalation of Na^+, and Ni^{4+} with strong oxidation oxidizes electrolyte and tends to self-decomposition. As shown in Figure 4b, High-nickel cathode material of SIBs or LIBs has a high specific capacity, but it also shows unsatisfactory thermal stability. The regulation of structure and composition is an effective way to improve the thermal stability of cathode materials. Sun et al. reported a concentration-gradient cathode with high Ni content in core and high Mn content in shell.[99] The high-Ni core ensures a high capacity while the inactive Mn^{4+} at the surface promotes the thermal stability. Meanwhile, reducing the content of Ni or Co in metal oxides can further improve the thermal stability of bulk structure. Sun's group comprehensively studied the decomposition temperature of O3-type layered $Na[Ni_xCo_yMn_z]O_2$ (x = 1/3, 0.5, 0.6, and 0.8) cathodes at a highly desodiated state and the highest decomposition temperature (310.7 °C) and the lowest heat release (306.4 J g^{-1}) occur when x = 1/3.[100] This work states that the electrochemical, structural and thermal properties of O3 type layered cathode are strongly dependent on the composition of transition metals. Accordingly, it is not to be neglected to balance the physico-chemical role of each transition metal in a new microstructure design for the development of thermally stable cathode materials.

In addition, the thermal stability of the cathode could be improved by overall substituting Ni by Cr, Ti, Mn and other thermal-stable elements (Figure 4b). P3-phase $Na_{0.5}CrO_2$ has unobvious heat release performance in organic electrolytes[101], which was more stable than charged layered (Na)$LiCoO_2$.[102]

Yabuuchi et al. reported an in-plane distorted P3-type $Na_{0.5}CrO_2$ and observed the oxygen loss only above 500 °C with the formation of Cr_2O_3 and $NaCrO_2$ as stable phases, making it a potentially safe positive electrode material for SIBs.[101] Zhao et al. studied the thermal stability of α-$NaFeO_2$ by thermogravimetry coupled with differential scanning calorimeter and compared with that of LCO.[103] Thermal decomposition of $Na_{0.58}FeO_2$ powder occurs at a temperature higher than 300 °C and the mixture with electrolyte undergoes exothermic reaction in the range of 220–300 °C. Compared with LCO, $NaFeO_2$ showed less total heat generation and higher initial exothermic temperature.

It is essential to find substitutable electrode materials with thermally stable bulk structure because the intrinsic thermal property of layered oxides still raises the safety concern. Polyanion compounds cathode materials have obvious superiority over Na_xTMO_2 cathode materials in thermal stability aspect (Figure 4b). NASICON-type phosphate-based host provides structural stability due to strong covalent $(PO_4)^{3-}$ units even at high SOC and surmounts thermal safety concerns (excessive heat generation, self-decomposition at high temperature, oxygen evolution, etc.). The iron-based phosphate incline to decompose in the range of 500 – 550 °C to form various pyrophosphate-based products such as $NaFeP_2O_7$, $Na_4P_2O_7$, $Fe_{1.5}P_2O_7$, and so forth.[104–108] Kim et al. investigated the thermal stability of $NaFe_3(PO_4)_2(P_2O_7)$ by in situ high-temperature XRD, which demonstrated that this compound decomposed into $NaFeP_2O_7$ and $Fe_2P_2O_7$ due to breaking of $(PO_4)^{3-}$ in 530 °C.[106] Therefore, the pyrophosphate anion is considered energetically more thermally stable than $(PO_4)^{3-}$ at high temperature. Barpanda et al. reported a novel $Na_{2-x}FeP_2O_7$ (x = 0, 1) material to deliver stability up to 600 °C, making pyrophosphate become a strong competitor for practical application of safe and economical SIBs system.[108] Besides, carbon with an excellent electronic conductivity can be utilized to tackle the poor conductivity of phosphate, thus it could show a high overall capacity even under high current density after modification. Furthermore, $Na_2Fe_2(SO_4)_3$,[109] $Na_3(VO_{1-x}PO_4)_2F_{1+2x}$ ($0 \leq x \leq 1$),[110–111] and Na_2FeSiO_4[112–113] also displayed higher thermal decomposition temperature and less heat release, compared with Na_xTMO_2. Guan et al. demonstrated a high-safety and low-cost cathode material Na_2FeSiO_4 for SIBs.[112] The TG and DSC results confirmed that the fully desodiated carbon-coated Na_2FeSiO_4 was thermal stable up to 800 °C, except for the decomposition of the carboxymethylcellulose sodium adhesive at 230–450 °C. Besides, sodium terephthalate with high decomposition temperature of 640 °C could potentially resolve safety problems of thermal abuse[114].

3.3. Nonflammable Electrolyte

In a Na-ion battery, electrolyte is just as critical as the blood system of a human body, associating with various components. However, it has been regarded as the weakest part to resist the heat generation and diffusion. Due to its flammability and high electrochemical reduction activity, the traditional nonaqueous electrolyte brings safety problems under abusive conditions.

**ADVANCED
SCIENCE NEWS**
www.advancedsciencenews.com

**ADVANCED
ENERGY
MATERIALS**
www.advenergymat.de

Therefore, reducing the chemical activity while maintaining the electrochemical properties of the electrolyte is an essential research topic. Water-in-salts electrolytes, ionic liquids, non-flammable organic electrolytes, and solid state electrolytes are regarded as promising electrolyte for high-safety SIBs.

Water-in-salt electrolyte is a type of aqueous electrolytes, obtained by dissolving sodium salt at extremely high concentration in water.[115] When the molar concentration of salt is higher than 5 M, the definition of water-in-salt is applicable. To settle down the problem of narrow decomposition voltage of water (1.23 V), the highly concentrated salts were added to greatly broaden the electrochemical window of aqueous electrolyte, thus realizing a higher energy density aqueous SIBs.[116–117] Jiang et al. developed a new water-in-salt electrolyte by jointly dissolving 22 M tetraethyl ammonium trifluoromethylsulfonate and 9 M sodium trifluoromethylsulfonate in water.[118] This novel electrolyte can not only achieve a wide electrochemical window of 3.3 V, but effectively inhibit the dissolution of $Na_{1.88}Mn(Fe(CN)_6)_{0.97} \cdot 1.35H_2O$ cathode materials during the cycling process. Suo et al. proposed a water-in-salt electrolyte based on $NaCF_3SO_3$ salt, which can form a Na^+ conductive SEI film on the surface of $NaTi_2(PO_4)_3$ anode, and suppress the hydrogen evolution reaction.[116] In addition, the reduced hydro-chemical activity also hinders the oxygen evolution reaction on the $Na_{0.66}[Mn_{0.66}Ti_{0.34}]O_2$ cathode to obtain a 2.5 V electrochemical stable window. Water-in-salt electrolytes are intrinsically nonflammable, showing the superiority of high safety and environmental friendliness, however, the expensive price and relatively low electrochemical window are considered as critical issues to be solved.[119]

Ionic liquids (ILs) have characteristics of low volatility, high ionic conductivity, good thermal stability, low flammability, and wide electrochemical stability window,[120] making ILs-based battery systems highly thermochemical stable. Typical ILs include imidazolium, piperidine, pyrrole, and inorganic ILs, etc.[29] Wang et al. dissolved $NaBF_4$, $NaClO_4$, $NaPF_6$, and NaTFSI into butylmethylpyrrolidinium-bis(trifluoromethanesulfonyl) imide (BMPTFSI) ILs and used them as electrolytes in the $Na_{0.44}MnO_2$/Na battery.[121] It showed that $NaClO_4$/BMPTFSI-based battery exhibited the lowest SEI film formation impedance and charge-transfer impedance. In addition, BMPTFSI decomposes at a relatively higher temperature of 400 °C compared with traditional organic solvents (less than 100 °C). Monti et al. found that imidazole-type ILs, e.g., NaTFSI/1-ethyl-3-methylimidazolium bis(trifluoromethylsulfonyl)imide (NaTFSI/EMIm-TFSI) and NaTFSI/1-butyl-3-methylimidazolium-TFSI (NaTFSI/BMIm-TFSI) maintain good stability up to 150 °C.[122] The high price and instability against carbon anode materials impedes the practical use of ILs in SIBs. Mixed electrolyte with organic solvent and ILs may be able to achieve a balanced performance.

Besides, the incombustible organic electrolyte has a certain application prospect in terms of high ionic conductivity, good wettability at electrode surface, and wide voltage window. Non-flammable organic electrolytes are mainly classified into three types: phosphates electrolyte, highly concentrated electrolytes (HCE) and localized HCE.

Phosphorus, as a fire-retardant element, greatly reduces the SET and promotes the application of organic phosphate additives/electrolytes in SIBs. According to the chemical structures, the traditional phosphates can be divided into linear and cyclic phosphates (**Figure 5**a). The linear phosphates include trimethyl phosphate (TMP),[86,123] triethyl phosphate (TEP),[124–125] dimethyl methylphosphonate (DMMP),[126–127] diethyl ethylphosphonate (DEEP),[128] etc. The cyclic phosphates contain ethoxy-(pentafluoro)-cyclotriphosphazene (PFN),[129] 9,10-Dihydro-9-oxa-10-phosphaphenanthrene-10-oxide (DOPO),[130] hexakis(2,2,2-trifluoroethoxy)cyclotriphosphazene (HFEPN),[131] etc. Those organic phosphates have predominance of low viscosity, wide application temperature range and high dielectric constant. The mechanism for the flame retardation of organic-phosphorus compounds is to be a chemical radical-scavenging process (Figure 5b).[132] At elevated temperature, the phosphorus flame retardant produces free radical inhibitors R• and H•, which could capture the free radicals or oxygen that promote the growth of combustion reaction. Finally, a thermal hysteresis layer is formed, covering the surface of the electrode, thus interrupting the combustion chain reaction. The thermal behaviors of the same electrode material in different electrolytes reflect the flammability difference of the electrolytes. As shown in Figure 5c, $NaTi_2(PO_4)_3$ and $NaV_2(PO_4)_3$ materials displayed less heat release and higher reaction temperature in TMP organic phosphate electrolyte than that of EC-DMC (dimethyl carbonate) electrolyte ($NaTi_2(PO_4)_3$ in TMP: 94.8 J g^{-1} and 417.4 °C; $NaTi_2(PO_4)_3$ in EC-DMC: 106.2 J g^{-1} and 295.4 °C; $NaV_2(PO_4)_3$ in TMP: 234 J g^{-1} and 333.9 °C; $NaV_2(PO_4)_3$ in EC-DMC: 240.8 J g^{-1} and 323.3 °C), demonstrating more fire-retardant effect in phosphate electrolytes.[86,133] In addition, the investigation of $NaV_2(PO_4)_3$ cathode and Na_xC in various electrolytes also lead to the same conclusion.[86,133] However, these organic phosphates decompose seriously on the anode, which dramatically deteriorate the electrochemical performance.[123,133] In order to tackle this issue, adding the film forming additives or fluoroalkyl phosphates are proved for effective SEI formation in anode materials. Liu et al. displayed a symmetric SIB using $Na_3V_2(PO_4)_3$ as electrode material along with TEP solvent dissolving 0.9 M $NaClO_4$ as the nonflammable electrolyte.[125] This incombustible TEP not only ensures the overall safety of the battery, but also shows excellent rate performance (35.1 mA h g^{-1} at 32 °C) and excellent cycle performance. Zeng et al. reported a TMP electrolyte with FEC additive (0.8 M $NaPF_6$/TMP + 10 vol% FEC), showing a suitable thermal safety and good compatibility with Sb/Na anode. A high initial capacity of 490 mA h g^{-1} is achieved for full cells composed of Sb-based anode and $NaNi_{0.35}Mn_{0.35}Fe_{0.3}O_2$ cathode.[123] Jiang et al. applied tris(2,2,2-trifluoroethyl) phosphate (TFEP, one form of fluoroalkyl phosphates) to form a stable inorganic-enriched SEI for its low decomposition barrier, ensuring a high capacity retention of hard carbon anode.[133] Moreover, the charged $NaV_2(PO_4)_3$ and Na_xC in the presence of TFEP shows a relatively lower exothermic temperature and less heat release than that in carbonate electrolyte, illustrating both nonflammability characteristic and extremely low exothermic properties. Overall, phosphate electrolytes, compared with conventional carbonate electrolytes, pave a novel trail for developing safe SIBs.

Advanced electrolytes have been investigated to overcome the thermal safety of SIBs, and HCE is as one of the representatives.[134–135] Difference from the diluted electrolytes, most
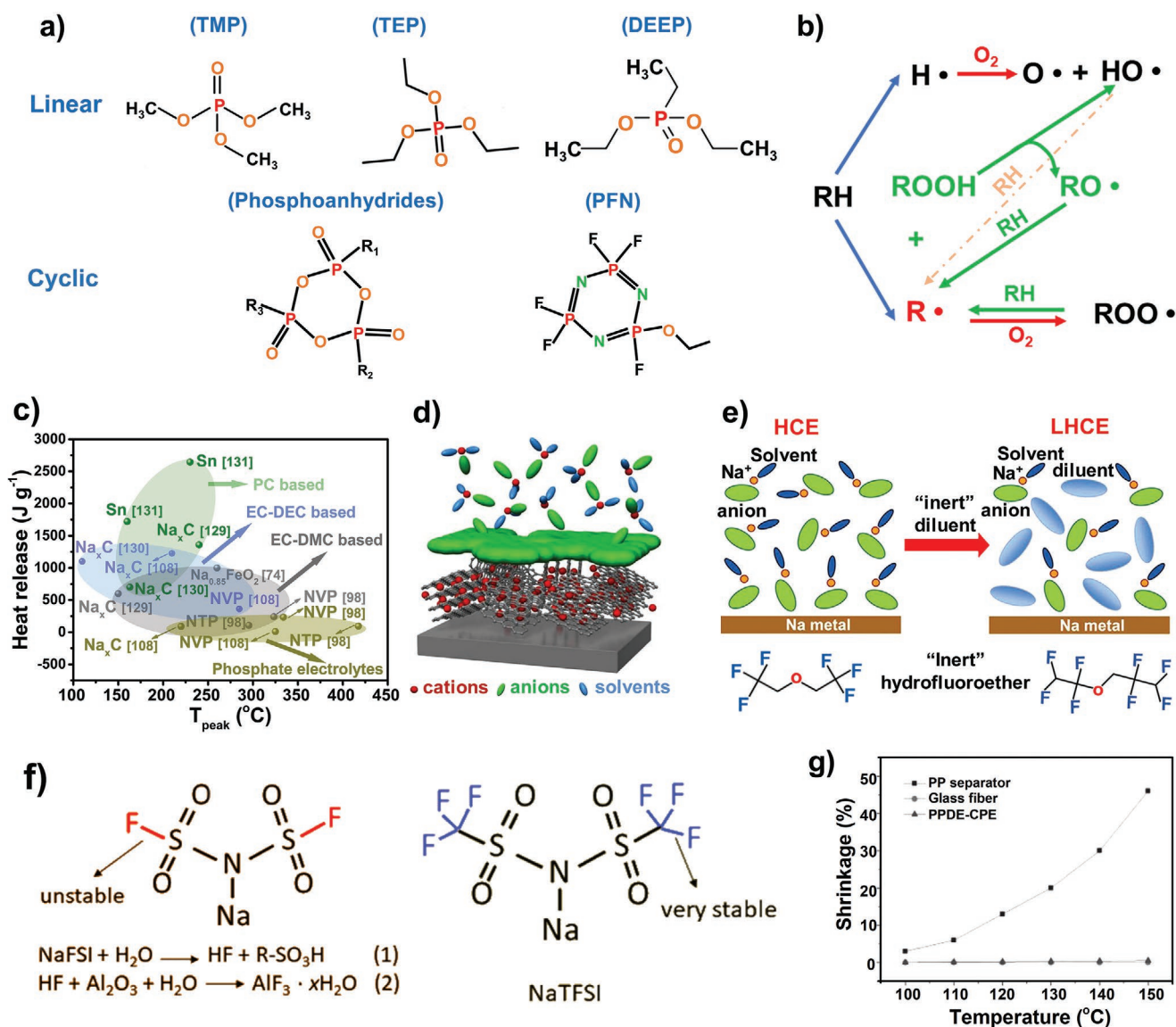
ADVANCED
SCIENCE NEWS

www.advancedsciencenews.com

ADVANCED
ENERGY
MATERIALS

www.advenergymat.de

Figure 5. a) Chemical structures of some representative organophosphates. b) Flame retardant mechanism of organophosphate. c) The exothermic temperature and total heat of various electrode materials in PC-/EC-DEC-/EC-DMC-based electrolytes and phosphate electrolytes (NTP: $NaTi_2(PO_4)_3$; $NaV_2(PO_4)_3$).[86,92,103,133,175–176] d) Intercalation behavior of cations into a carbonaceous anode in nonflammable concentrated electrolyte. Reproduced with permission.[137] Copyright 2017, Nature Publishing Group. e) Schematic illustration of the dilution process from a HCE to a LHCE, and representative chemical structure of hydrofluoroether. Reproduced with permission.[139] Copyright 2018, American Chemical Society. f) Chemical structure of the NaFSI (left) and the NaTFSI (right). Reproduced with permission.[151] Copyright 2019, American Chemical Society. g) Thermal shrinkage ratio from 100 to 150 °C of PP separator, glass fiber, and poly(ethylene glycol) divinyl ether based polymer electrolyte (PPDE-CPE). Reproduced with permission.[152] Copyright 2016, Wiley-VCH.

of the solvent molecules form solvation pairs with Na⁺ in the HCE system, which decreases the number of free solvent molecules.[136] As a consequence, the activity and flammability of the electrolyte are suppressed due to lack of free solvent molecules, and anions can be preferentially recruited in the solvation sheath of Na⁺ ions. Therefore, it leads to the decomposition of anions in preference to the solvent, and formation of anion-derived fluorinated SEI, which remarkably distinguishes with conventional dilute electrolyte (Figure 5d).[137] Since the anion drives the formation of SEI layer, the components in the SEI are mainly composed by inorganic salts. These inorganics

are believed to accelerate the diffusion of Na⁺ and strengthen the mechanical property of SEI. The presence of this special SEI layer weakens the growth of dendrite, inhibits the corrosion of Al current collectors, and widens the electrochemical stability window of SIBs. More importantly, the abuse temperature of thermal runaway can be further increased. Wang et al. demonstrated that a concentrated electrolyte with 3.3 M NaFSA in TMP organic solvent for SIBs allows stable cycling of both hard carbon and graphite anodes for more than 1,000 cycles with negligible degradation.[137] It shows negligible volatility up to 150 °C for the concentrated 3.3 M NaFSA/TMP. According

**ADVANCED
SCIENCE NEWS**
www.advancedsciencenews.com

**ADVANCED
ENERGY
MATERIALS**
www.advenergymat.de

to density functional theory molecular dynamics simulation, most of the TMP molecules are coordinated with Na^+ and more than 80% of the FSA^- anions are in an aggregate state in HCE, leading to a nonflammable electrolyte with zero SET because of the disappear of free solvent. The charge-discharge test also shows an improved ICE of 75%.

Nevertheless, the poor wettability to separator, high viscosity, and high cost of HCE caused by increased concentration will obstruct the application of SIBs. The localized highly concentrated electrolytes (LHCE) have been investigated to overcome this issue.[138] Adding inert diluent (such as hydrofluoroether) to the HCE system is able to preserve the structure of solvated pairs (Figure 5e).[139] It possesses wide electrochemical stable voltage window as well as low viscosity. LHCE electrolyte is in a metastable state due to inert diluent is miscible with HCE but do not dissolve any sodium salts. The concentration of electrolyte is one of the most critical influence factors on the price of electrolyte. Li et al. reported an ultra-low salt concentration electrolyte by dissolving 0.3 M $NaPF_6$ in EC/PC (1:1 in vol%) to reduce the electrolyte cost and expand the operation temperature range (−30 to 55 °C).[140] The dilute electrolyte chemistry provides a new path for rechargeable batteries under extreme operation conditions. Future research should focus on the trade-off among the safety, electronic conductivity, temperature adaptability, and the price of electrolytes.

Further, functional additives, such as redox shuttle additives, can improve the battery safety by protecting the battery from overcharging. Ji et al. reported a new organic salt, triaminocyclopropene perchlorate (TAC·ClO_4), as a redox shuttle in SIBs.[141] Under overcharge conditions, the charge potential is steadily locked at 3.75 V by a reversible oxidation-diffusion-reduction process between TAC cation and dication. The initiation potential of TAC oxidation is 0.2 V higher than the end-of-charge potential of $Na_3V_2(PO_4)_3$ cathode, which can perfectly ensure the normal operation of a battery. Even under harsh conditions, e.g., 400% SOC or at a high rate of 10 C, TAC can still effectively avoid voltage increase with a low concentration of 0.1 M.

Solid state electrolytes (SSE) have been regarded as the ultimate solution for developing high-energy and high-safety SIBs. SSE can be generally divided into inorganic ceramic/glass electrolytes, organic polymer electrolytes and ceramic-polymer composite electrolytes.[142] SSE have the advantage of good thermal stability, low flammability, good durability and simple battery design.[143–145] However, the room temperature ionic conductivity of solid electrolyte is still lower than that of liquid electrolyte. In addition, the problems of metal dendrite, price, interface stability and physical contact are also the main problems related to electrolyte in solid-state batteries.[146–148] Goodenough's group reported the application of a plastic-crystal electrolyte interface composed of succinonitrile and sodium salt.[149] $N≡C(CH_2)_2C≡N$ molecules are orderly arranged into lattice, but they show fluctuating degrees of freedom, which promotes the charge separation of different metal salts. The introduction of a plastic-crystal electrolyte interface between the solid electrolyte and the solid cathode reduces the interface resistance by about 4 times, increases the cycle life and ensures high rate performance. In addition, Goodenough's team employed ceramic solid electrolyte to optimize $Na_2MnFe(CN)_6$/Na system.[147] This novel NASICON

solid electrolyte reduces the manufacturing cost, constructs a stable interface of low impedance, and restrains the side reaction under high potential and the dissolution of transition metal ions. On the premise of improving the safety performance, the electrochemical performance is guaranteed. Nevertheless, there still are several scientific problems and technical challenges in the Na | SSE interface. Of course, the technical basis of artificial SEI or mixed solid electrolyte needs to be further explored. Solid polymer electrolytes (SPE) have shown evident advantages of high flexibility, low cost, facile processing, and good interface compatibility.[150] However, low ionic conductivity, excess free solvent molecules, and weak mechanical strength still limit its application. Liu et al. proposed an in situ approach to remove the residual free water molecules in SPE through a spontaneous chemical reaction.[151] The hydrolysis process of NaFSI salt consumes H_2O and generates HF, and HF further reacts with the added Al_2O_3 or SiO_2 nanoparticles to form stable hydrates (Figure 5f). The as-prepared SPE can effectively reduce the interface side reactions of solid-state batteries and greatly improve the coulombic efficiency, cycle stability and rate performance of batteries. Besides, decomposition temperatures of this as-prepared $PEO_{20}NaFSI + x$ wt% Al_2O_3 ($x = 0, 1, 2$) blended polymer electrolyte are all higher than 265 °C. Zhang et al. synthesized polysulfonamide-supported poly(ethylene glycol) divinyl ether based polymer electrolyte via an in situ polymerization method.[152] This polymer electrolyte exhibits relatively high ionic conductivity (1.2 mS cm^{-1}) at ambient temperature and favorable mechanical strength (25 MPa), which provides a new pathway for high-performance as well as high safety polymer electrolyte toward SIBs (Figure 5g). Goodenough's group proposed a preparation of a thermally-stable composite gel–polymer/glass–fiber electrolyte with PVDF-HFP strengthened by a glass–fiber (GF) and coated by polydopamine (PDA) for SIBs.[153] This composite polymer matrix-GF/PVDF-HFP/PDA exhibits superior mechanical strength (20.9 MPa) and stability up to 200 °C. (**Figure 6**a)

3.4. Thermal Shutdown Materials

Thermal shutdown materials, a class of temperature responsive materials, are frequently applied in LIBs.[154–156] Analogously, these strategies can be transferred into the design of safe SIBs, including thermal response membranes, electrolytes, and polymer monomer additives, etc. (Figure 6b,c) Thermal shutdown is general realized by the resistance change from the polymerization of small molecules, or the melting of diaphragm[157–158] during the temperature increase process to terminate the operation of battery. These functional materials have to meet the following requirements: 1) high conductivity at room temperature and large resistance change rate; 2) appropriate resistance change temperature (i.e., Curie temperature) or polymerization/melting temperature; 3) high chemical and electrochemical stability and good compatibility with each component of the battery. Some temperature-responsive electrolyte components are promising for thermal control. Thermopolymerization monomer could polymerize at elevated temperature to
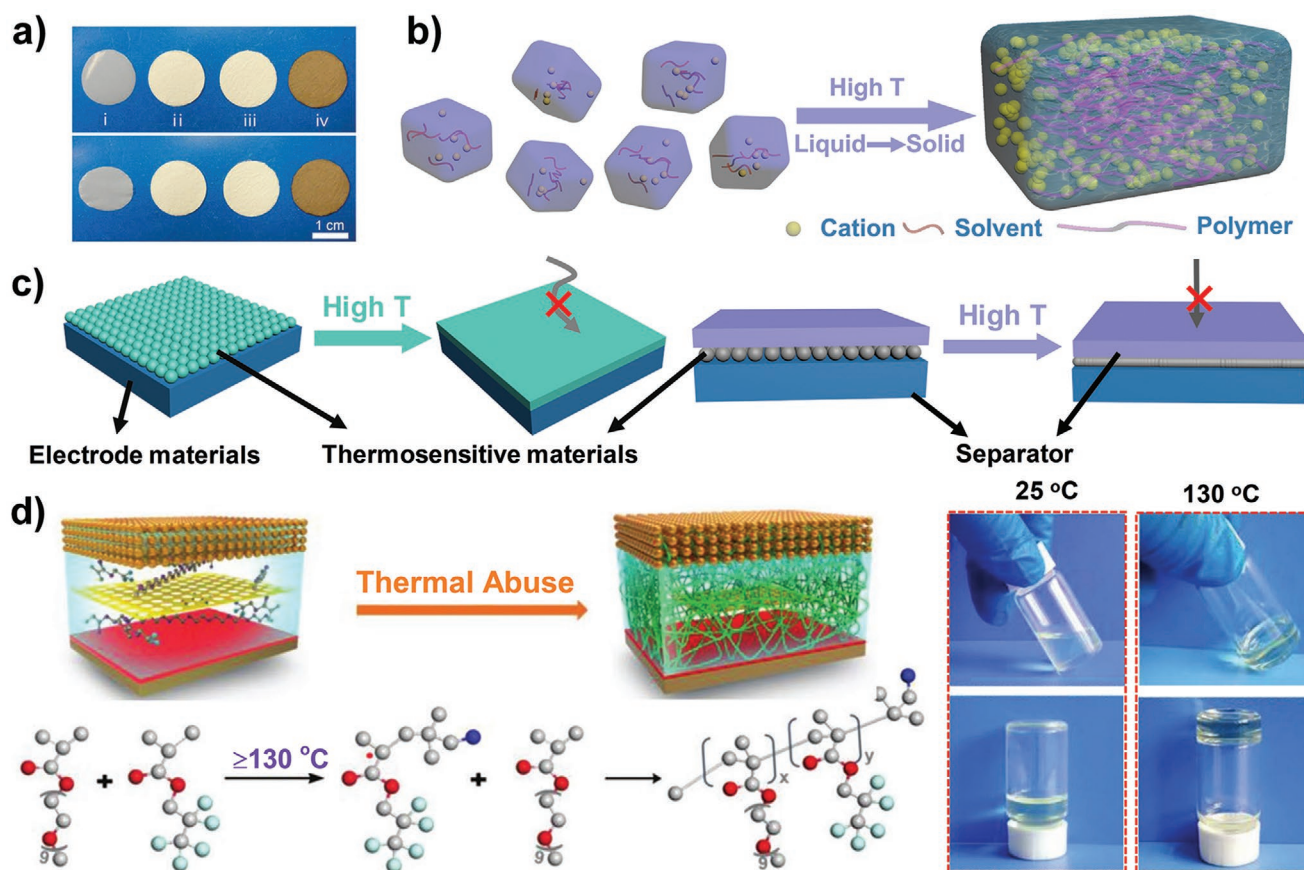
**ADVANCED
SCIENCE NEWS**
www.advancedsciencenews.com

**ADVANCED
ENERGY
MATERIALS**
www.advenergymat.de

Figure 6. a) Photographs of i) Celgard separator, ii) glass fiber, iii) GF/PVDF-HFP, and iv) GF/PVDF-HFP/PDA at room temperature (top) and after thermal treatment at 200 °C for 30 min (bottom). Reproduced with permission.[153] Copyright 2015, Wiley-VCH. b) Schematic diagram of the high temperature self-polymerized electrolyte as thermal shutdown material. c) Schematic diagram of thermal response coating and diaphragm. d) Schematic illustration of smart temperature-responsive electrolyte's (PPE's) thermal responsive behavior in cell and the corresponding free radical polymerization mechanism under thermal abuse condition, and optical photographs of PPE at 25 °C and after 130 °C thermal abuse. Reproduced with permission.[166] Copyright 2019, Wiley-VCH.

increase impedance of the electrolyte system and shut down the battery before the HTR loop starts. Typical thermopolymerization monomers include organic metallic locenes, divinyl ether, oxitane, dimethacrylate-based derivatives, etc.[159–163]

Baginska et al. incorporated thermoresponsive polymer microspheres onto battery anodes and separators to achieve autonomic, thermally-induced shutdown.[164] Polyethylene (PE) and paraffin microspheres spin-coated on the graphite anode melted at elevated temperatures (110 °C for PE and 65 °C for paraffin), and formed ≈20 µm thick film on the cycled anode, which blocks the ions diffusion and leads to an autonomous shutdown under some abuse conditions (Figure 6c). Hence, suitable polymer materials with temperature sensitivity can adjust the temperature of thermal shutdown, which is of great significance for SIBs. Gao et al. modified the separator structure of PE chain by solid-state ultraviolet (UV) irradiation.[165] About 40% of the crystalline PE chains completely melted and filled the pores at 130 °C. Meanwhile, due to its highly crosslinked structure, polyethylene separator can maintain its integrity to 220 °C and the partially crosslinked polyethylene membrane has hydrophilicity (33° of the contact angles with water), being instrumental in absorbing more electrolytes.

Another feasible method is to select the thermosensitive polymer monomer as the electrolyte additive for alkaline metal

ion battery. By stimulating the polymerization at a certain temperature, thermal runaway can be avoided. When the internal temperature of the battery increases, the polymerizable monomer additives will undergo thermal crosslinking polymerization, and this process can transform the electrolyte from the liquid to the gel state, weakening or even blocking the diffusion of ions between the cathode and anode, and terminating the electrode reaction to provide overheating protection for battery (Figure 6b). Zhou et al. proposed a smart temperature responsive electrolyte by adding poly(ethylene glycol) methyl ether methacrylate and 2,2,3,3,3-pentafluoropropyl acrylate mixture (Figure 6d).[166] The stable solid electrolyte interface was created by anionic polymerization with the initiation of lithium metal, leading to a reversible long-time cycling and dendrite-free anode. At the beginning of thermal runaway process, the electrolyte will rapidly solidify through thermal radical polymerization, so that the battery is stable at 150 °C even up to 280 °C. In principle, the thermal polymerization temperature of the monomer additive is slightly higher than the maximum normal use temperature of the battery, but lower than the minimum prohibited use temperature. Then, the thermal crosslinking polymerization speed of the monomer additive at high temperature is fast enough to ensure that the electrode reaction can

**ADVANCED
SCIENCE NEWS**
www.advancedsciencenews.com

**ADVANCED
ENERGY
MATERIALS**
www.advenergymat.de

be effectively blocked in time. Finally, it is requested to have high electrochemical matching to avoid adverse effects on the normal electrochemical performance of the battery. The development of this type of thermosensitive materials will provide an effective strategy for the future development of safe SIBs.

Materials with thermal-responsive physical properties have the potential to reversibly shutdown and recover the battery at a designed temperature. Chen et al. reported a reversible thermoresponsive polymer composite film composed of graphene-coated nickel nanoparticles GrNi filler and polymer matrix with a high thermal expansion coefficient.[167] The electronic conductivity of polymer composite film is up to 50 s cm^{-1} at room temperature and the conductivity decreases by 7 to 8 orders of magnitude once reaching the transition temperature and recovers at room temperature. Li et al. proposed poly(3-octylpyrrole): poly(styrenesulfonate) (P3OPy: PSS)/carbon composite (P3OPy/C) as a new positive temperature coefficient (PTC) material.[168] The resistance of cathode material LiCoO$_2$ mixed with P3OPy/C suddenly jumps to $1.3 \times 10^4 \Omega$ cm when the temperature rises to 100–120 °C, which is more than 4 times higher than that at ambient temperature.

4. Conclusions and Perspective

This work summarizes the major heat generation source, the electrochemical/chemical reactions occur during thermal runaway process, and recent progress of materials design for high safety SIBs. Minimizing Q_p and Q_s, accelerating the heat transport rate, flame retardants, and thermal shutdown materials would be effective directions to prevent fire or explosion accidents. The irreversible heat Q_p, generated because of the voltage polarizations, could be reduced by accelerating electrons and Na$^+$ ions mobility among electrodes and interfaces, which is also the prerequisite for a good electrochemical reaction kinetics. In addition, to achieve fast heat transportation, an efficient conductive network for phonons, which is the major carrier for heat conduction, should be also integrated into the materials design without blocking Na$^+$ and e$^-$ transportation. Materials with less defects and grain boundaries, e.g., (pseudo) single crystal cathode materials, are expected to enhance the structural/interfacial stability and improve thermal conductivity. Another potentially feasible way is to build a 3D current collector with high electronic and thermal conductivity, e.g., carbon nanotubes, graphene, metal, etc. simultaneously reducing Q_p and increasing thermal conductivity.

In terms of lowering Q_s, the materials design concept mainly includes two aspects: enhancing the thermal stability of SEI through the innovation of electrolyte compositions or additives and improving the thermal stability of materials to minimizing heat generation from self-decomposition and oxygen evolution. Advanced cathode materials without lattice oxygen, such as Prussian White with a representative formula of Na$_2$FeFe(CN)$_6$, is expected to eliminate the production of oxygen and inhibit the combustion inside batteries.

Furthermore, making the SIBs intrinsically nonflammable and inexplosive would be the ultimate goal. Relative to water-in-salt and solid-state electrolytes, nonflammable organic electrolyte could combine the advantages of high energy density and rapid mass transfer at the electrode-electrolyte interface. The price of electrolytes is also an important factor that must be considered in SIBs. A reversible thermal responsive polymer switch, which could be applied in form of electrolyte additive, binders, coating layers on electrodes, separators, and current collectors, is a good way to protect the battery from thermal runaway under abuse conditions, such as internal short circuit and overheating.

The melting point of separators is also crucial for battery safety. Note that commercial thermal shutdown separators designed to delay or prevent thermal runaway process in LIBs may not be feasible in SIBs because of the poor wettability caused by evident difference in electrolyte compositions. As a result, developing novel separators with high wettability, low-resistance, low-cost, and high melting point are highly demanded in SIBs. A future research direction is to develop ceramic/polymer composite separators, including surface modification with ceramic coating and ceramic nanoparticle fillers.

At present, the study on thermochemistry of SIBs is still at a preliminary stage, which calls for more efforts in fundamental study on the thermal failure mechanism to provide more information to guide materials design. For example, theory modeling is highly desired to determine the amount of generated heat from different types of materials, components, and batteries, different in terms of battery electrochemistry, capacities, charge/discharge rates, working temperatures, etc. More experiments should be carried out to determine the key parameters for a thermal runaway process from materials, cells, modules, and packs levels to give a comprehensive evaluation of a Na-ion battery. Battery safety is a complicated problem involved with many influence factors and should be considered from a holistic point of view. In addition to materials design discussed in this work, other innovations in cell engineering and thermal management system are of equal importance to achieve a high-safety performance.

Conflict of Interest

The authors declare no conflict of interest.

**ADVANCED
SCIENCE NEWS**

www.advancedsciencenews.com

**ADVANCED
ENERGY
MATERIALS**

www.advenergymat.de

[1] T. Liu, Y. Zhang, Z. Jiang, X. Zeng, J. Ji, Z. Li, X. Gao, M. Sun, Z. Lin, M. Ling, *Energy Environ. Sci.* **2019**, *12*, 1512.

[2] J.-Y. Hwang, S.-T. Myung, Y.-K. Sun, *Chem. Soc. Rev.* **2017**, *46*, 3529.

[3] C. Vaalma, D. Buchholz, M. Weil, S. Passerini, *Nat. Rev. Mater.* **2018**, *3*, 18013.

[4] J. L. Murray, *Bull. Alloy Phase Diagrams* **1983**, *4*, 407.

[5] J. Barker, C. J. Wright, (Faradion Ltd), US20170237270A1, **2017**.

[6] X. Xia, J. Dahn, *Electrochem. Solid-State Lett.* **2011**, *15*, A1.

[7] J. B. Robinson, D. P. Finegan, T. M. Heenan, K. Smith, E. Kendrick, D. J. Brett, P. R. Shearing, *J. Electrochem. Energy Convers. Storage* **2018**, *15*, 011010.

[8] Y. Li, Y. Lu, L. Chen, Y.-S. Hu, *Chin. Phys. B* **2020**, *29*, 048201.

[9] Y. B. Niu, Y. X. Yin, Y. G. Guo, *Small* **2019**, *15*, e1900233.

[10] Y. Li, Y. Lu, P. Adelhelm, M. M. Titirici, Y. S. Hu, *Chem. Soc. Rev.* **2019**, *48*, 4655.

[11] Y. Li, Y. Lu, C. Zhao, Y. S. Hu, M. M. Titirici, H. Li, X. Huang, L. Chen, *Energy Storage Mater.* **2017**, *7*, 130.

[12] A. Ponrouch, D. Monti, A. Boschin, B. Steen, P. Johansson, M. R. Palacín, *J. Mater. Chem. A* **2015**, *3*, 22.

[13] Y. Xie, G.-L. Xu, H. Che, H. Wang, K. Yang, X. Yang, F. Guo, Y. Ren, Z. Chen, K. Amine, *Chem. Mater.* **2018**, *30*, 4909.

[14] X. Xia, J. Dahn, *J. Electrochem. Soc.* **2012**, *159*, A1048.

[15] K. Liu, Y. Liu, D. Lin, A. Pei, Y. Cui, *Sci. Adv.* **2018**, *4*, eaas9820.

[16] J. Wen, Y. Yu, C. Chen, *Mater. Express* **2012**, *2*, 197.

[17] A. Nazari, S. Farhad, *Appl. Therm. Eng.* **2017**, *125*, 1501.

[18] V. Dusastre, *Materials for Sustainable Energy*, Nature Publishing Group, World Scientific, Hackensack, NJ **2011**.

[19] R. Spotnitz, J. Franklin, *J. Power Sources* **2003**, *113*, 81.

[20] G. Karimi, X. Li, *Int. J. Energy Res.* **2013**, *37*, 13.

[21] P. Valenciajr , C.-C. Hsu, A. M. Bilinski, R. M. Brisbane, (GM Global Technology Operations LLC), US10230140B2, **2019**.

[22] Y. Huo, Z. Rao, X. Liu, J. Zhao, *Energy Convers. Manage.* **2015**, *89*, 387.

[23] G. Liu, M. Ouyang, L. Lu, J. Li, X. Han, *J. Therm. Anal. Calorim.* **2014**, *116*, 1001.

[24] D. Bernardi, E. Pawlikowski, J. Newman, *J. Electrochem. Soc.* **1985**, *132*, 5.

[25] Y. Ye, Y. Shi, N. Cai, J. Lee, X. He, *J. Power Sources* **2012**, *199*, 227.

[26] P. Amiribavandpour, W. Shen, D. Mu, A. Kapoor, *J. Power Sources* **2015**, *284*, 328.

[27] X. Li, T. Wang, L. Pei, C. Zhu, B. Xu, in *A Comparative Study of Sorting Methods for Lithium-Ion Batteries, 2014 IEEE Conf. and Expo Transportation Electrification Asia-Pacific (ITEC Asia-Pacific)*, IEEE, Beijing, China **2014**.

[28] Y. Saito, *J. Power Sources* **2005**, *146*, 770.

[29] Y. Sun, P. Shi, H. Xiang, X. Liang, Y. Yu, *Small* **2019**, *15*, 1805479.

[30] C.-F. Chen, A. Verma, P. P. Mukherjee, *J. Electrochem. Soc.* **2017**, *164*, E3146.

[31] K. Onda, T. Ohshima, M. Nakayama, K. Fukuda, T. Araki, *J. Power Sources* **2006**, *158*, 535.

[32] Y. Lai, S. Du, L. Ai, L. Ai, Y. Cheng, Y. Tang, M. Jia, *Int. J. Hydrogen Energy* **2015**, *40*, 13039.

[33] T. M. Bandhauer, S. Garimella, T. F. Fuller, *J. Power Sources* **2014**, *247*, 618.

[34] W. Fang, O. J. Kwon, C. Y. Wang, *Int. J. Energy Res.* **2010**, *34*, 107.

[35] R. Kantharaj, A. M. Marconnet, *Nanoscale Microscale Thermophys. Eng.* **2019**, *23*, 128.

[36] J. Liu, M. Kunz, K. Chen, N. Tamura, T. J. Richardson, *J. Phys. Chem. Lett.* **2010**, *1*, 2120.

[37] G. G. Eshetu, T. Diemant, M. Hekmatfar, S. Grugeon, R. J. Behm, S. Laruelle, M. Armand, S. Passerini, *Nano Energy* **2019**, *55*, 327.

[38] X. Liu, D. Ren, H. Hsu, X. Feng, G.-L. Xu, M. Zhuang, H. Gao, L. Lu, X. Han, Z. Chu, *Joule* **2018**, *2*, 2047.

[39] X. Wu, K. Song, X. Zhang, N. Hu, L. Li, W. Li, L. Zhang, H. Zhang, *Front. Energy Res.* **2019**, *7*, 65.

[40] D. P. Finegan, M. Scheel, J. B. Robinson, B. Tjaden, I. Hunt, T. J. Mason, J. Millichamp, M. Di Michiel, G. J. Offer, G. Hinds, *Nat. Commun.* **2015**, *6*, 6924.

[41] S. Hess, M. Wohlfahrt-Mehrens, M. Wachtler, *J. Electrochem. Soc.* **2015**, *162*, A3084.

[42] H. Xiang, H. Xu, Z. Wang, C. Chen, *J. Power Sources* **2007**, *173*, 562.

[43] H. Ji, L. Zhang, M. T. Pettes, H. Li, S. Chen, L. Shi, R. Piner, R. S. Ruoff, *Nano Lett.* **2012**, *12*, 2446.

[44] W. Luo, P. Zhang, X. Wang, Q. Li, Y. Dong, J. Hua, L. Zhou, L. Mai, *J. Power Sources* **2016**, *304*, 340.

[45] S. Shi, L. Liu, C. Ouyang, D.-s. Wang, Z. Wang, L. Chen, X. Huang, *Phys. Rev. B* **2003**, *68*, 195108.

[46] W. Shen, H. Li, C. Wang, Z. Li, Q. Xu, H. Liu, Y. Wang, *J. Mater. Chem. A* **2015**, *3*, 15190.

[47] Y. Teng, H. Zhao, Z. Zhang, L. Zhao, Y. Zhang, Z. Li, Q. Xia, Z. Du, K. Świerczek, *Carbon* **2017**, *119*, 91.

[48] I. V. Thorat, D. E. Stephenson, N. A. Zacharias, K. Zaghib, J. N. Harb, D. R. Wheeler, *J. Power Sources* **2009**, *188*, 592.

[49] J. S. Cho, J.-S. Park, Y. C. Kang, *Nano Res.* **2017**, *10*, 897.

[50] Y.-H. Zhu, Q. Zhang, X. Yang, E.-Y. Zhao, T. Sun, X.-B. Zhang, S. Wang, X.-Q. Yu, J.-M. Yan, Q. Jiang, *Chem* **2019**, *5*, 168.

[51] S. Chen, C. Wu, L. Shen, C. Zhu, Y. Huang, K. Xi, J. Maier, Y. Yu, *Adv. Mater.* **2017**, *29*, 1700431.

[52] W. J. Lv, Z. Huang, Y. X. Yin, H. R. Yao, H. L. Zhu, Y. G. Guo, *ChemNanoMat* **2019**, *5*, 1253.

[53] H. Kim, H. Kim, Z. Ding, M. H. Lee, K. Lim, G. Yoon, K. Kang, *Adv. Energy Mater.* **2016**, *6*, 1600943.

[54] M. Okubo, E. Hosono, T. Kudo, H. Zhou, I. Honma, *J. Phys. Chem. Solids* **2008**, *69*, 2911.

[55] P. Klemens, *Proc. R. Soc. London, Ser. A* **1951**, *208*, 108.

[56] L. Yang, Z. G. Chen, M. S. Dargusch, J. Zou, *Adv. Energy Mater.* **2018**, *8*, 1701797.

[57] K. Fujita, T. Mochida, K. Nakamura, *Jpn. J. Appl. Phys.* **2001**, *40*, 4644.

[58] J. Li, X. Zuo, X. Zhao, J. Ouyang, H. Yang, *Appl. Clay Sci.* **2019**, *173*, 12.

[59] M. Kazan, P. Masri, *Surf. Sci. Rep.* **2014**, *69*, 1.

[60] L. Liang, B. Li, *Phys. Rev. B* **2006**, *73*, 153303.

[61] Y. Dong, B.-Y. Cao, Z.-Y. Guo, *Phys. E* **2014**, *56*, 256.

[62] T. Terao, C. Zhi, Y. Bando, N. Mitome, C. Tang, D. Golberg, *J. Phys. Chem. C* **2010**, *114*, 4340.

[63] W. Cui, F. Du, J. Zhao, W. Zhang, Y. Yang, X. Xie, Y.-W. Mai, *Carbon* **2011**, *49*, 495.

[64] Q. Yao, L. Chen, W. Zhang, S. Liufu, X. Chen, *ACS Nano* **2010**, *4*, 2445.

[65] Z. Wu, H. Xie, *Mater. Res. Innovations* **2013**, *18*, 120.

[66] M. Dahbi, N. Yabuuchi, M. Fukunishi, K. Kubota, K. Chihara, K. Tokiwa, X.-f. Yu, H. Ushiyama, K. Yamashita, J.-Y. Son, *Chem. Mater.* **2016**, *28*, 1625.

[67] H. Lu, L. Wu, L. Xiao, X. Ai, H. Yang, Y. Cao, *Electrochim. Acta* **2016**, *190*, 402.

[68] T. Yim, S. H. Kim, S.-G. Woo, K. Lee, J. H. Song, W. Cho, K. J. Kim, J.-S. Kim, Y.-J. Kim, *RSC Adv.* **2014**, *4*, 19172.

[69] I. A. Profatilova, C. Stock, A. Schmitz, S. Passerini, M. Winter, *J. Power Sources* **2013**, *222*, 140.

[70] X. Chen, X. Li, D. Mei, J. Feng, M. Y. Hu, J. Hu, M. Engelhard, J. Zheng, W. Xu, J. Xiao, *ChemSusChem* **2014**, *7*, 549.

[71] L. Ji, M. Gu, Y. Shao, X. Li, M. H. Engelhard, B. W. Arey, W. Wang, Z. Nie, J. Xiao, C. Wang, *Adv. Mater.* **2014**, *26*, 2901.

[72] J. Zheng, H. Zheng, R. Wang, L. Ben, W. Lu, L. Chen, L. Chen, H. Li, *Phys. Chem. Chem. Phys.* **2014**, *16*, 13229.

[73] N. Weadock, N. Varongchayakul, J. Wan, S. Lee, J. Seog, L. Hu, *Nano Energy* **2013**, *2*, 713.

[74] C. Bommier, X. Ji, *Small* **2018**, *14*, 1703576.

[75] J. Song, B. Xiao, Y. Lin, K. Xu, X. Li, *Adv. Energy Mater.* **2018**, *8*, 1703082.

[76] G. G. Eshetu, S. Grugeon, H. Kim, S. Jeong, L. Wu, G. Gachot, S. Laruelle, M. Armand, S. Passerini, *ChemSusChem* **2016**, *9*, 462.

[77] Y. Li, Y. Lu, Q. Meng, A. C. S. Jensen, Q. Zhang, Q. Zhang, Y. Tong, Y. Qi, L. Gu, M. M. Titirici, Y. S. Hu, *Adv. Energy Mater.* **2019**, *9*, 1902852.

[78] Y. Zhao, K. R. Adair, X. Sun, *Energy Environ. Sci.* **2018**, *11*, 2673.

[79] L. Fan, X. Li, *Nano Energy* **2018**, *53*, 630.

[80] Y. Liu, D. Lin, P. Y. Yuen, K. Liu, J. Xie, R. H. Dauskardt, Y. Cui, *Adv. Mater.* **2017**, *29*, 1605531.

[81] G. G. Eshetu, G. A. Elia, M. Armand, M. Forsyth, S. Komaba, T. Rojo, S. Passerini, *Adv. Energy Mater.* **2020**, https://doi.org/10.1002/aenm.202000093.

[82] J. Xiao, *Science* **2019**, *366*, 426.

[83] Q. Shi, Y. Zhong, M. Wu, H. Wang, H. Wang, *Angew. Chem., Int. Ed.* **2018**, *130*, 9207.

[84] S. Wei, S. Choudhury, J. Xu, P. Nath, Z. Tu, L. A. Archer, *Adv. Mater.* **2017**, *29*, 1605512.

[85] X. Wu, Y. Cao, X. Ai, J. Qian, H. Yang, *Electrochem. Commun.* **2013**, *31*, 145.

[86] X. Jiang, Z. Zeng, L. Xiao, X. Ai, H. Yang, Y. Cao, *ACS Appl. Mater. Interfaces* **2017**, *9*, 43733.

[87] Y. Niu, M. Xu, C. Guo, C. M. Li, *J. Colloid Interface Sci.* **2016**, *474*, 88.

[88] Y. Kong, J. Sun, L. Gai, X. Ma, J. Zhou, *Electrochim. Acta* **2017**, *255*, 220.

[89] Y. Ge, H. Jiang, K. Fu, C. Zhang, J. Zhu, C. Chen, Y. Lu, Y. Qiu, X. Zhang, *J. Power Sources* **2014**, *272*, 860.

[90] A. Rudola, K. Saravanan, S. Devaraj, H. Gong, P. Balaya, *Chem. Commun.* **2013**, *49*, 7451.

[91] C. Wu, Z.-G. Wu, X. Zhang, R. Rajagopalan, B. Zhong, W. Xiang, M. Chen, H. Li, T. Chen, E. Wang, *ACS Appl. Mater. Interfaces* **2017**, *9*, 43596.

[92] Y. Lee, H. Lim, S.-O. Kim, H.-S. Kim, K. J. Kim, K.-Y. Lee, W. Choi, *J. Mater. Chem. A* **2018**, *6*, 20383.

[93] L. Shao, Q. Zhao, J. Chen, *Chem. Commun.* **2017**, *53*, 2435.

[94] S.-L. Chou, Y. Pan, J.-Z. Wang, H.-K. Liu, S.-X. Dou, *Phys. Chem. Chem. Phys.* **2014**, *16*, 20347.

[95] A. Ponrouch, A. Goñi, M. R. Palacín, *Electrochem. Commun.* **2013**, *27*, 85.

[96] L. Zhu, H. Hou, D. Zhao, S. Liu, W. Ye, S. Chen, M. Hanif, *Int. J. Electrochem. Sci.* **2015**, *10*, 9547.

[97] Z. Zhengming John, *Chem. Rev.* **2004**, *104*, 4419.

[98] Y. Ansari, B. Guo, J. H. Cho, K. Park, J. Song, C. J. Ellison, J. B. Goodenough, *J. Electrochem. Soc.* **2014**, *161*, A1655.

[99] Y. K. Sun, D. H. Kim, C. S. Yoon, S. T. Myung, J. Prakash, K. Amine, *Adv. Funct. Mater.* **2010**, *20*, 485.

[100] J.-Y. Hwang, C. S. Yoon, I. Belharouak, Y.-K. Sun, *J. Mater. Chem. A* **2016**, *4*, 17952.

[101] N. Yabuuchi, I. Ikeuchi, K. Kubota, S. Komaba, *ACS Appl. Mater. Interfaces* **2016**, *8*, 32292.

[102] W. Huang, A. Marcelli, D. Xia, *Adv. Energy Mater.* **2017**, *7*, 1700460.

[103] J. Zhao, L. Zhao, N. Dimov, S. Okada, T. Nishida, *J. Electrochem. Soc.* **2013**, *160*, A3077.

[104] H. Kim, R. Shakoor, C. Park, S. Y. Lim, J. S. Kim, Y. N. Jo, W. Cho, K. Miyasaka, R. Kahraman, Y. Jung, *Adv. Funct. Mater.* **2013**, *23*, 1147.

[105] F. Yang, H. Gao, J. Chen, Z. Guo, *Small Methods* **2017**, *1*, 1700216.

[106] H. Kim, I. Park, D.-H. Seo, S. Lee, S.-W. Kim, W. J. Kwon, Y.-U. Park, C. S. Kim, S. Jeon, K. Kang, *J. Am. Chem. Soc.* **2012**, *134*, 10369.

[107] P. Moreau, D. Guyomard, J. Gaubicher, F. Boucher, *Chem. Mater.* **2010**, *22*, 4126.

[108] P. Barpanda, G. Liu, C. D. Ling, M. Tamaru, M. Avdeev, S.-C. Chung, Y. Yamada, A. Yamada, *Chem. Mater.* **2013**, *25*, 3480.

[109] M. Chen, D. Cortie, Z. Hu, H. Jin, S. Wang, Q. Gu, W. Hua, E. Wang, W. Lai, L. Chen, *Adv. Energy Mater.* **2018**, *8*, 1800944.

[110] S. Liu, L. Wang, J. Liu, M. Zhou, Q. Nian, Y. Feng, Z. Tao, L. Shao, *J. Mater. Chem. A* **2019**, *7*, 248.

[111] C. Chen, T. Li, H. Tian, Y. Zou, *J. Mater. Chem. A* **2019**, *7*, 18451.

[112] W. Guan, B. Pan, P. Zhou, J. Mi, D. Zhang, J. Xu, Y. Jiang, *ACS Appl. Mater. Interfaces* **2017**, *9*, 22369.

[113] B. Ali, F. Ghafoor, M. I. Shahzad, S. K. Shah, S. M. Abbas, *J. Power Sources* **2018**, *396*, 467.

[114] Y. Park, D. S. Shin, S. H. Woo, N. S. Choi, K. H. Shin, S. M. Oh, K. T. Lee, S. Y. Hong, *Adv. Mater.* **2012**, *24*, 3562.

[115] L. Suo, O. Borodin, T. Gao, M. Olguin, J. Ho, X. Fan, C. Luo, C. Wang, K. Xu, *Science* **2015**, *350*, 938.

[116] L. Suo, O. Borodin, Y. Wang, X. Rong, W. Sun, X. Fan, S. Xu, M. A. Schroeder, A. V. Cresce, F. Wang, *Adv. Energy Mater.* **2017**, *7*, 1701189.

[117] D. P. Leonard, Z. Wei, G. Chen, F. Du, X. Ji, *ACS Energy Lett.* **2018**, *3*, 373.

[118] L. Jiang, L. Liu, J. Yue, Q. Zhang, A. Zhou, O. Borodin, L. Suo, H. Li, L. Chen, K. Xu, *Adv. Mater.* **2020**, *32*, 1904427.

[119] M. R. Lukatskaya, J. I. Feldblyum, D. G. Mackanic, F. Lissel, D. L. Michels, Y. Cui, Z. Bao, *Energy Environ. Sci.* **2018**, *11*, 2876.

[120] Q. Yang, Z. Zhang, X.-G. Sun, Y.-S. Hu, H. Xing, S. Dai, *Chem. Soc. Rev.* **2018**, *47*, 2020.

[121] C.-H. Wang, Y.-W. Yeh, N. Wongittharom, Y.-C. Wang, C.-J. Tseng, S.-W. Lee, W.-S. Chang, J.-K. Chang, *J. Power Sources* **2015**, *274*, 1016.

[122] D. Monti, E. Jónsson, M. R. Palacín, P. Johansson, *J. Power Sources* **2014**, *245*, 630.

[123] Z. Zeng, X. Jiang, R. Li, D. Yuan, X. Ai, H. Yang, Y. Cao, *Adv. Sci.* **2016**, *3*, 1600066.

[124] H. Yang, Q. Li, C. Guo, A. Naveed, J. Yang, Y. Nuli, J. Wang, *Chem. Commun.* **2018**, *54*, 4132.

[125] X. Liu, X. Jiang, F. Zhong, X. Feng, W. Chen, X. Ai, H. Yang, Y. Cao, *ACS Appl. Mater. Interfaces* **2019**, *11*, 27833.

[126] J. Feng, Z. Zhang, L. Li, J. Yang, S. Xiong, Y. Qian, *J. Power Sources* **2015**, *284*, 222.

[127] H. Xiang, Q. Wang, D. Wang, D. Zhang, H. Wang, C. Chen, *J. Appl. Electrochem.* **2011**, *41*, 965.

[128] J. Feng, P. Ma, H. Yang, L. Lu, *Electrochim. Acta* **2013**, *114*, 688.

[129] J. Liu, X. Song, L. Zhou, S. Wang, W. Song, W. Liu, H. Long, L. Zhou, H. Wu, C. Feng, *Nano Energy* **2018**, *46*, 404.

[130] J. Zheng, X. Li, Y. Yu, X. Feng, Y. Zhao, *J. Therm. Anal. Calorim.* **2014**, *117*, 319.

[131] C. K. Kim, D. S. Shin, K. E. Kim, K. Shin, J. J. Woo, S. Kim, S. Y. Hong, N. S. Choi, *ChemElectroChem* **2016**, *3*, 913.

[132] E.-G. Shim, T.-H. Nam, J.-G. Kim, H.-S. Kim, S.-I. Moon, *Electrochim. Acta* **2007**, *53*, 650.

[133] X. Jiang, X. Liu, Z. Zeng, L. Xiao, X. Ai, H. Yang, Y. Cao, *iScience* **2018**, *10*, 114.

[134] C. Geng, D. Buchholz, G. T. Kim, D. V. Carvalho, H. Zhang, L. G. Chagas, S. Passerini, *Small Methods* **2019**, *3*, 1800208.

[135] J. Patra, H.-T. Huang, W. Xue, C. Wang, A. S. Helal, J. Li, J.-K. Chang, *Energy Storage Mater.* **2019**, *16*, 146.

[136] Y. Yamada, J. Wang, S. Ko, E. Watanabe, A. Yamada, *Nat. Energy* **2019**, *4*, 269.

[137] J. Wang, Y. Yamada, K. Sodeyama, E. Watanabe, K. Takada, Y. Tateyama, A. Yamada, *Nat. Energy* **2018**, *3*, 22.

[138] C. C. Su, M. He, R. Amine, K. Amine, *Angew. Chem., Int. Ed.* **2019**, *131*, 1051.

[139] J. Zheng, S. Chen, W. Zhao, J. Song, M. H. Engelhard, J.-G. Zhang, *ACS Energy Lett.* **2018**, *3*, 315.

[140] Y. Li, Y. Yang, Y. Lu, Q. Zhou, X. Qi, Q. Meng, X. Rong, L. Chen, Y.-S. Hu, *ACS Energy Lett.* **2020**, *5*, 1156.

[141] W. Ji, H. Huang, X. Zhang, D. Zheng, T. Ding, T. H. Lambert, D. Qu, *Nano Energy* **2020**, https://doi.org/10.1016/j.nanoen.2020.104705.

**ADVANCED
SCIENCE NEWS**

www.advancedsciencenews.com

**ADVANCED
ENERGY
MATERIALS**

www.advenergymat.de

[142] Y. Wang, S. Song, C. Xu, N. Hu, J. Molenda, L. Lu, *Nano Mater. Sci.* **2019**, *1*, 91.

[143] M. Armand, J.-M. Tarascon, *Nature* **2008**, *451*, 652.

[144] J. J. Kim, K. Yoon, I. Park, K. Kang, *Small Methods* **2017**, *1*, 1700219.

[145] C. Zhao, L. Liu, X. Qi, Y. Lu, F. Wu, J. Zhao, Y. Yu, Y. S. Hu, L. Chen, *Adv. Energy Mater.* **2018**, *8*, 1703012.

[146] L. Zhang, K. Yang, J. Mi, L. Lu, L. Zhao, L. Wang, Y. Li, H. Zeng, *Adv. Energy Mater.* **2015**, *5*, 1501294.

[147] H. Gao, S. Xin, L. Xue, J. B. Goodenough, *Chem* **2018**, *4*, 833.

[148] W. Zhou, H. Gao, J. B. Goodenough, *Adv. Energy Mater.* **2016**, *6*, 1501802.

[149] H. Gao, L. Xue, S. Xin, K. Park, J. B. Goodenough, *Angew. Chem., Int. Ed.* **2017**, *56*, 5541.

[150] J. Yang, H. Zhang, Q. Zhou, H. Qu, T. Dong, M. Zhang, B. Tang, J. Zhang, G. Cui, *ACS Appl. Mater. Interfaces* **2019**, *11*, 17109.

[151] L. Liu, X. Qi, S. Yin, Q. Zhang, X. Liu, L. Suo, H. Li, L. Chen, Y.-S. Hu, *ACS Energy Lett.* **2019**, *4*, 1650.

[152] J. Zhang, H. Wen, L. Yue, J. Chai, J. Ma, P. Hu, G. Ding, Q. Wang, Z. Liu, G. Cui, L. Chen, *Small* **2017**, *13*, 1601530.

[153] H. Gao, B. Guo, J. Song, K. Park, J. B. Goodenough, *Adv. Energy Mater.* **2015**, *5*, 1402235.

[154] L. Xia, D. Wang, H. Yang, Y. Cao, X. Ai, *Electrochem. Commun.* **2012**, *25*, 98.

[155] L. Kong, B. Liu, J. Ding, X. Yan, G. Tian, S. Qi, D. Wu, *J. Membr. Sci.* **2018**, *549*, 244.

[156] K. Chen, C. L. Schmidt, P. M. Skarstad (Medtronic Inc), *US8945753B2*, **2015**.

[157] C. J. Orendorff, T. N. Lambert, C. A. Chavez, M. Bencomo, K. R. Fenton, *Adv. Energy Mater.* **2013**, *3*, 314.

[158] E. S. Takeuchi, Thermal protection separator for alkali metal batteries, *Google Patents*, **2002**.

[159] M. N. Golovin, D. P. Wilkinson, J. T. Dudley, D. Holonko, S. Woo, *J. Electrochem. Soc.* **1992**, *139*, 5.

[160] C. Buhrmester, L. Moshurchak, R. L. Wang, J. Dahn, *J. Electrochem. Soc.* **2006**, *153*, A288.

[161] S. Chen, W. D. Cook, F. Chen, *Polym. Int.* **2007**, *56*, 1423.

[162] W. Z. Xia, W. D. Cook, *Polymer* **2003**, *44*, 79.

[163] J. R. Nair, I. Shaji, N. Ehteshami, A. Thum, D. Diddens, A. Heuer, M. Winter, *Chem. Mater.* **2019**, *31*, 3118.

[164] M. Baginska, B. J. Blaiszik, R. J. Merriman, N. R. Sottos, J. S. Moore, S. R. White, *Adv. Energy Mater.* **2012**, *2*, 583.

[165] X. Gao, W. Sheng, Y. Wang, Y. Lin, Y. Luo, B. G. Li, *J. Appl. Polym. Sci.* **2015**, *132*, 42169.

[166] Q. Zhou, S. Dong, Z. Lv, G. Xu, L. Huang, Q. Wang, Z. Cui, G. Cui, *Adv. Energy Mater.* **2020**, *10*, 1903441.

[167] Z. Chen, P.-C. Hsu, J. Lopez, Y. Li, J. W. To, N. Liu, C. Wang, S. C. Andrews, J. Liu, Y. Cui, *Nat. Energy* **2016**, *1*, 15009.

[168] H. Li, F. Wang, C. Zhang, W. Ji, J. Qian, Y. Cao, H. Yang, X. Ai, *Energy Storage Mater.* **2019**, *17*, 275.

[169] H. Dai, C. Yang, X. Ou, X. Liang, H. Xue, W. Wang, G. Xu, *Electrochim. Acta* **2017**, *257*, 146.

[170] S. Y. Lim, H. Kim, R. Shakoor, Y. Jung, J. W. Choi, *J. Electrochem. Soc.* **2012**, *159*, A1393.

[171] J. Zhao, J. Xu, D. H. Lee, N. Dimov, Y. S. Meng, S. Okada, *J. Power Sources* **2014**, *264*, 235.

[172] H. Xu, S. Xie, Q. Wang, X. Yao, Q. Wang, C. Chen, *Electrochim. Acta* **2006**, *52*, 636.

[173] W. Tang, Z. Chen, F. Xiong, F. Chen, C. Huang, Q. Gao, T. Wang, Z. Yang, W. Zhang, *J. Power Sources* **2019**, *412*, 246.

[174] A. K. Padhi, K. S. Nanjundaswamy, J. B. Goodenough, *J. Electrochem. Soc.* **1997**, *144*, 1188.

[175] J. Zhao, L. Zhao, K. Chihara, S. Okada, J.-i. Yamaki, S. Matsumoto, S. Kuze, K. Nakane, *J. Power Sources* **2013**, *244*, 752.

[176] A. Ponrouch, E. Marchante, M. Courty, J.-M. Tarascon, M. R. Palacin, *Energy Environ. Sci.* **2012**, *5*, 8572.

2000974 (17 of 17)